



Published in final edited form as:

Nat Microbiol. 2024 February ; 9(2): 561–575. doi:10.1038/s41564-023-01581-x.

High-throughput transcriptomics of 409 bacteria-drug pairs reveals drivers of gut microbiota perturbation

Deirdre Ricaurte^{1,2,#}, Yiming Huang^{1,2,#}, Ravi U. Sheth^{1,2}, Diego Rivera Gelsinger¹, Andrew Kaufman¹, Harris H. Wang^{1,3,*}

¹Department of Systems Biology, Columbia University, New York, NY, USA.

²Integrated Program in Cellular, Molecular, and Biomedical Studies, Columbia University, New York, NY, USA.

³Department of Pathology and Cell Biology, Columbia University, New York, NY, USA.

Abstract

Many drugs can perturb the gut microbiome, potentially leading to negative health consequences. However, mechanisms of most microbe-drug responses have not been elucidated at the genetic level. Using high-throughput bacterial transcriptomics, we systematically characterized the gene expression profiles of prevalent human gut bacteria exposed to the most frequently prescribed orally administered pharmaceuticals. Across >400 drug-microbe pairs, significant and reproducible transcriptional responses were observed, including pathways involved in multidrug resistance, metabolite transport, tartrate metabolism, and riboflavin biosynthesis. Importantly, we discovered that statin-mediated upregulation of the AcrAB-TolC efflux pump in *Bacteroidales* species enhances microbial sensitivity to vitamin A and secondary bile acids. Moreover, gut bacteria carrying *acrAB-tolC* genes are depleted in patients taking simvastatin, suggesting that drug-efflux interactions generate collateral toxicity that depletes pump-containing microbes from patient microbiomes. This work provides a resource to further understand the drivers of drug-mediated microbiota shifts for better informed clinical interventions.

Today, half of all Americans take at least one prescription drug, with national spending predicted to reach \$400 billion by 2025^{1,2}. The prevalent use of pharmaceuticals is a major contributor to the alarming shifts in the gut microbiome, especially in industrialized countries^{3,4}. A recent screen of >1,000 orally administered drugs revealed a high

*Correspondences should be addressed to harris.wang@columbia.edu.

#These authors contributed equally.

AUTHOR CONTRIBUTIONS STATEMENT

D.R., Y.H., R.U.S., and H.H.W. developed the initial concepts; D.R. and Y.H. performed experiments and analyzed data with assistance from A.K., D.R.G and R.U.S. and input from H.H.W.; D.R., Y.H., and H.H.W. wrote the manuscript. All other authors discussed results and approved the manuscript.

CODE AVAILABILITY

Scripts used to analyze sequencing data in this study can be accessed at https://github.com/wanglabcumc/microbial_RNAseq_processing.

COMPETING INTERESTS STATEMENT

H.H.W. is a scientific advisor of SNIPR Biome, Kingdom Supercultures, Fitbiomics, Arranta Bio, VecX Biomedicines, Genus PLC, and a scientific co-founder of Aclid, all of whom are not involved in the study. R.U.S is a co-founder of Kingdom Supercultures. The authors declare no additional competing interests.

frequency of antibacterial activity among human-targeted medications (24%), especially antipsychotics⁵. Clinically, proton pump inhibitors and atypical antipsychotics often trigger microbiota changes, with side-effects resembling those of antibiotic use (e.g., diarrhea, fungal infection)^{5,6}. Even though the top three prescribed drug classes (i.e., antihyperlipidemic agents, antidepressants, analgesics⁷) are all linked to gut microbiota disturbances, the mechanisms driving these shifts are poorly understood⁵. Physiologically, altered microbiome composition can negatively impact epithelial integrity⁸, gut motility⁹, nutrient availability¹⁰, immune homeostasis^{11,12}, and even treatment response. For instance, depletions in gut bacterial diversity have been linked to worse outcomes in immunotherapy drug trials¹³ and higher susceptibility to infection by pathogens such as *Clostridiodes difficile*¹⁴.

Gut microbes interact with pharmaceutical compounds in a variety of ways. Bacteria can biotransform drugs to impact efficacy^{15,16}, bioavailability¹⁷, and toxicity¹⁸. For example, commensal *Eggerthella lenta* inactivates digoxin, an orally delivered cardiac glycoside, by expressing the cardiac glycoside reductase (*cgr*) operon¹⁵. Gut bacteria can also deplete xenobiotics from their local environment via bioaccumulation¹⁹ and mitigate the effects of toxic medications by employing conserved antibiotic resistance mechanisms⁵. Within minutes of xenobiotic exposure, microbes often exhibit highly specific transcriptional responses^{20,21}. Therefore, transcriptomic measurements can help quickly dissect specific drug-microbe responses (e.g., digoxin¹⁵, 5-fluorouracil²², and levodopa²³). However, current cost and scale of bacterial transcriptomics has precluded high-throughput studies using this approach²⁴.

Here, we describe the systematic transcriptomic analysis of 409 drug-microbe pairs to dissect gene-level gut bacterial responses to top pharmaceuticals. We developed a high-throughput transcriptomics pipeline for optimization in non-model gut microorganisms that was then applied to generate a total of 978 individual drug-microbe samples (including replicates). By analyzing the transcriptomes of prevalent human gut bacteria exposed to top-prescribed orally administered drugs, we observed shared and strain-specific responses, including in pathways for drug degradation, vitamin biosynthesis, and multidrug efflux. Further analysis of a human microbiome cohort dataset confirmed the clinical significance of our findings. This study highlights the utility of large-scale transcriptomics for functional discovery of gut microbiota-xenobiotic interactions.

RESULTS

Transcriptomic map of microbial responses to top medicines

Of the top 200 drugs prescribed today, 83% are orally delivered and expected to interact directly with the gut microbiome^{5,25,26}. We therefore sought to measure the transcriptomic responses of prevalent gut bacteria exposed to top-prescribed oral pharmaceuticals. We implemented and optimized a multiplexed RNA-seq technique²⁷ for high-throughput transcriptomics of non-model gut bacteria and incorporated cost-efficient ribosomal RNA (rRNA) depletion for diverse non-model gut bacteria that we previously developed²⁴ (Fig. 1a). This modified pipeline can generate high-quality transcriptomes for diverse gut bacterial phyla at a cost of <\$16 for ~1M reads per sample (Supplementary Table 1).

We assembled a panel of 14 representative and highly prevalent^{28–30} human gut isolates spanning the *Bacteroidetes*, *Firmicutes*, *Actinobacteria*, and *Proteobacteria* phyla (see Supplementary Fig. 1, Supplementary Tables 2 & 3) and 19 oral drugs from the top prescribed drugs in 2017 according to the Agency for Healthcare Research and Quality (Supplementary Table 4, Methods)³¹. Our drug list included the top 8 most prescribed drugs as well as 10 additional neurotransmitter modulators, which were included due to established associations between the psychotherapeutic drug class and microbiota compositional changes⁵. Lenalidomide, a chemotherapeutic with the largest market cap in the small molecule drug class³¹, was also added.

We first assessed the antimicrobial activity of the chosen drugs against our bacterial panel (Fig. 1b, Supplementary Fig. 2; Methods). Drug concentrations were chosen to span median drug concentrations within the small and large intestine, which have been estimated to approach 20 and 100 μM , respectively⁵. We did not observe growth inhibition for most strains at 2 or 20 μM concentrations (Supplementary Fig. 2). At 100 μM , growth inhibition was observed for at least one drug in 18 of 19 strains within 24 hours (Fig. 1b). Notably, *B. longum* did not exhibit growth defects in any drug condition. Broad spectrum antimicrobial activity was seen for simvastatin, amlodipine, and a subset of psychotherapeutics (i.e., sertraline, paroxetine, duloxetine, fluoxetine), in agreement with previous reports⁵. Interestingly, we observed the greatest magnitudes of drug-induced growth defects within *Bacteroidetes* strains, suggesting that these species are more susceptible to drug toxicities (Fig. 1b, Supplementary Fig. 2). We further validated that the observed toxicity profiles extended to complex bacterial communities by exposing the drug panel to a fresh fecal sample from a healthy volunteer. We observed similar growth inhibition profiles of 13 panel strains grown in fecal community (Supplementary Fig. 3), supporting the relevance of our individual strain-level growth measurements in the context of a complex consortium.

Since substantial growth inhibition can confound transcriptional measurements, we performed all subsequent transcriptomic assays at 20 μM , which reasonably approximated intestinal drug concentrations for detecting drug responses while minimizing drug toxicities^{5,32}. To further avoid impact of antimicrobial toxicity, cells were harvested at 1.5 hours post-exposure, which is shorter than the doubling time of several gut bacteria³³. The transcriptomic pipeline was first validated using *Eggerthella lenta* exposed to our drug panel, as well as digoxin as a positive control (Supplementary Figs. 4-5, Supplementary Table 5). Differential *E. lenta* gene expression was observed in 17 of 20 drug conditions, including the expected upregulation of the *cgr* operon by digoxin¹⁵ (Supplementary Fig. 5). The transcriptomic pipeline was thus applied to all drug-microbe pairs in biological duplicates (Supplementary Fig. 4b, Supplementary Tables 6-8).

Overall, substantial and consistent transcriptional responses were observed across drug classes and bacterial phyla (Supplementary Table 6). We used the magnitude of global transcriptional response as a common proxy³⁴ by calculating the ratio of differentially expressed genes (DEGs) to the total gene count per genome, which we refer to as the DEG ratio or DEGR (Fig. 1c). All drugs produced differential expression in at least one strain. The largest aggregate DEGR was produced by simvastatin (0.014), followed by sertraline

(0.010), levothyroxine (0.006), and paroxetine (0.004) (Fig. 1c, top bars). Notably, in many cases drugs eliciting large global transcriptional changes also exhibited broad-spectrum toxicity in the growth screen (Fig. 1b, c; Supplementary Fig. 6).

Large transcriptional changes are often associated with expression changes of global regulators and transcription factors (TFs)³⁵. Indeed, the drug-microbe pairings associated with the highest DEGRs (Simvastatin-*B. stercoris*, Sertraline-*F. saccharivorans*, Simvastatin-*A. shahii*) also induced the highest numbers of TFs (14, 13, and 12, respectively) (Supplementary Fig. 7). However, in several cases, bacterial-drug exposures generated differential expression without TF modulation, such as *D. longicatena* exposed to metoprolol tartrate and *P. dorei* exposed to various selective serotonin reuptake inhibitors (SSRIs) (Supplementary Fig. 7). In these cases, differential expression was not consistently correlated with antimicrobial activity (Fig. 1b, c). These results indicate that drug-microbe exposures producing large and broad gene expression changes often correlate with drug toxicity, while those eliciting specific transcriptional responses may not.

To understand the functional impact of different exposures on the gut microbiota, we performed pathway enrichment analysis using the KEGG (Kyoto Encyclopedia of Genes and Genomes) database to classify DEGs across the drug panel, agnostic of strain identity (Fig. 2). Most differentially regulated modules ($p_{\text{adj}} < 0.01$, $\text{FC} > 4$) were associated with mechanisms of antibiotic resistance (Fig. 2a). Specifically, pathways related to multidrug resistance, transport, and two-component systems were enriched. Simvastatin, sertraline, and amlodipine – the drugs exhibiting the broadest toxicity in growth screens – strongly upregulated multidrug resistance pathways associated with efflux transporters. Further, trazodone and levothyroxine, which triggered differential expression in *Bacteroidetes*, *Firmicutes*, and *Actinobacteria* without impacting growth (Fig. 1b, c), showed similarly enriched pathways to more toxic screened compounds (Fig. 2a). While growth deficits were not detected in trazodone and levothyroxine-treated cultures at the maximum concentrations, this result suggests that these compounds could exhibit toxicity *in vivo* at concentrations exceeding 100 μM . Notably, post-treatment microbiota changes have been detected in hypothyroid patients taking levothyroxine³⁶ and psychiatric patients taking trazodone³⁷.

We next examined functional orthologs within pathways that exhibited the greatest magnitudes of differential regulation across drug conditions (Fig. 2b). Among the top 7 most upregulated orthologs, 6 corresponded to conserved multidrug efflux pumps (Fig. 2b). Among these orthologs, the top 4 (HAE1, AcrA, mexK, oprM) belonged to the Resistance-Nodulation-Division (RND) permease superfamily, a drug and heavy metal efflux system whose upregulation is associated with gram-negative bacterial antibiotic resistance^{38,39}. The fifth and sixth orthologs (bcrB and ABCB-BAC) belonged to the ATP-binding cassette (ABC) superfamily, which was also highly represented among the top downregulated orthologs across drug conditions (Fig. 2b). Interestingly, the ABC superfamily is not considered to contribute substantially to bacterial multidrug resistance; however, these pumps are highly associated with chemotherapy resistance in eukaryotic cells⁴⁰. Together, these observations suggest that gut bacterial strains utilize conserved multidrug efflux pumps to ameliorate toxicities of human-targeted drug compounds⁵.

Given the link between the identified RND-type efflux pumps and antibiotic resistance in gram-negative species^{38,39}, we wondered whether gut bacteria employ the same resistance pathways to ameliorate toxicities in commonly prescribed antibiotic classes. To explore this question, we generated transcriptomes for 4 species (*A. rectalis* H1, *D. longicatena* H1, *B. longum* H1, *P. vulgatus* H1) exposed to 7 commonly prescribed antibiotics that target bacterial synthesis of DNA (ciprofloxacin), proteins (tetracycline, streptomycin, erythromycin), or the cell membrane (cefotaxime, ampicillin, vancomycin) (Supplementary Figs. 4 & 8, Supplementary Table 9). Principal coordinates analysis (PCoA) revealed that transcriptomic responses to traditional antibiotics clustered by drug target across sensitive strains (*A. rectalis*, *D. longicatena*, *P. vulgatus*), suggesting that bacteria utilize conserved pathways to mitigate toxicities of drugs with similar bacterial targets (Supplementary Fig. 8a). Notably, minimal transcriptomic responses to streptomycin exposures were observed, consistent with inherent streptomycin resistance of anaerobically grown bacterial isolates⁴¹. Further, *B. longum*, the only bacterial strain in our panel that did not exhibit growth sensitivity to at least one screened pharmaceutical, demonstrated minimal transcriptional responses to antibiotic exposures as compared to a vehicle control, a behavior consistent with resistance³². To compare bacterial pathways induced by traditional antibiotic exposures, we next performed a KEGG pathway enrichment analysis of DEGs in the 4 tested bacteria exposed to orally delivered drugs or traditional antibiotics (Supplementary Fig. 8b). Membrane-directed antibiotics upregulated pathways associated with cell membrane synthesis and modification (vancomycin resistance, fatty acid synthesis pathways), while ribosomal-targeted antibiotics induced upregulation of ribosomal pathways and downregulation of ATP-synthesis. Remarkably, our analysis revealed no overlap in bacterial pathways induced by non-antibiotic pharmaceuticals and traditional antibiotic compounds, suggesting that non-antibiotic orally delivered compounds impact unique mechanisms of prokaryotic multidrug resistance.

Drugs impact gut bioavailability, biosynthesis and toxicity

To obtain a deeper functional understanding of bacterial-drug interactions at the operon level, we searched for clusters of DEGs transcribed within the same operon. Numerous differentially expressed operons were identified across strains (Supplementary Table 8). Existing mechanistic studies of gut microbiota drug interactions have identified a range of bacterial drug responses that can cause differential treatment outcomes, including drug metabolism, toxicity mitigation and alteration of the prokaryotic metabolome^{5,19,42}. In order to explore the diversity of physiologically relevant bacterial xenobiotic interactions, we selected 3 representative operons associated with drug metabolism, vitamin biosynthesis, and toxicity mitigation for further examination (Fig. 3).

First, we observed upregulation of the tartrate dehydratase (*ttt*) operon in *E. coli*, *A. rectalis*, and *D. longicatena* exposed to metoprolol tartrate, a beta blocker used to treat hypertension⁴³ (Fig. 3a). Metoprolol is chemically formulated either as metoprolol tartrate or metoprolol succinate for immediate release or extended release, respectively. Which form of metoprolol is administered can impact bioavailability, with metoprolol tartrate producing higher peak-to-trough variation among patients⁴⁴. For bacteria, dietary tartrate metabolism through the *ttt* operon provides another carbon source in the gastrointestinal

tract⁴⁵. Our results suggest that certain gut microbes can metabolize the tartrate salt of immediate-release metoprolol, which could contribute to fluctuations in drug bioavailability within patient cohorts. These findings could also have broader implications for other tartrate-conjugated drugs⁴⁶. Furthermore, upregulation of tartrate metabolism by metoprolol could have unintended negative consequences in the context of cardiovascular disease⁴⁷. Increases in bacterial tartrate metabolism have been linked to metabolic disorders, including atherosclerotic cardiovascular disease (ACVD), type 2 diabetes (T2D) and obesity⁴⁷. Enrichment in tartrate metabolism has also been associated with higher abundance of *E. coli*, a metoprolol tartrate metabolizer identified in our screen. Using a published clinical metagenomic microbiome dataset of T2D patients⁴⁸, we performed an additional analysis exploring the distribution of *ttd* genes among T2D patients consuming metoprolol. We found that T2D patients taking metoprolol had an increased abundance of the *ttd* operon in their gut metagenome compared to patients not taking metoprolol ($p=0.046$) and healthy controls ($p=0.008$, Fig. 3b). Therefore, our findings combined with prior studies suggest that treatment with metoprolol tartrate for hypertension, which is the strongest predictor for ACVD⁴⁹, might inadvertently influence the pathophysiology of a metabolic disorder via an increase in microbiota tartrate metabolism.

Next, we identified differential regulation of the riboflavin biosynthesis (*rib*) operon in *D. longicatena* by several drugs within our panel (Fig. 3c). The gut microbiome is an important source of riboflavin (vitamin B2) in humans⁵⁰. Riboflavin production is an essential pathway in bacteria, as downstream metabolites flavin mononucleotide (FMN) and flavin adenine dinucleotide (FAD) are co-enzymes for oxidases, reductases, and dehydrogenases⁵¹. In gram-positive bacteria, riboflavin biosynthesis is downregulated by an FMN-responsive riboswitch, which also responds to roseoflavin⁵¹. In our transcriptomics dataset, several SSRIs (sertraline, paroxetine, fluoxetine, duloxetine), a cardiovascular medication (amlodipine), simvastatin, and levothyroxine all downregulate riboflavin production in *D. longicatena*. We also observed upregulation of the *rib* operon by *D. longicatena* in response to trazodone and atorvastatin exposure. Clinically, vitamin B2 deficiency is associated with higher risk of psychiatric disorders for which SSRIs are indicated (e.g., depression), though whether these depletions are a cause or a result of disease is not understood^{52,53}. Reduced riboflavin concentrations can also contribute to hyperhomocysteinemia, a well-studied independent risk factor for atherosclerosis^{54,55}. Our data suggest that the administration of certain SSRIs and cardiovascular medications could modulate vitamin B2 levels in the setting of mood disorders or heart disease, respectively, which could have unintended detrimental consequences on the disease state.

Finally, we observed a strong statin-mediated upregulation of genes encoding the AcrAB-TolC efflux pump in all *Bacteroidales* strains tested (*B. fragilis*, *B. stercoris*, *B. uniformis*, *P. dorei*, *P. vulgatus*, *P. distasonis*, *A. shahii*) (Fig 3d). The AcrAB-TolC pump has been linked to resistance against several classes of antibiotics as well as non-antibiotic orally delivered pharmaceuticals including methotrexate and tamoxifen^{5,56}. The pump is also known to mediate bacterial sensitivity to retinol and secondary bile acids⁵⁷. Given that previous studies have linked statin use with changes in gut microbiome composition²⁵, we thus explored the mechanism by which upregulation of AcrAB-TolC by statins could impact microbial physiology in the gut.

Statins modulate AcrAB-TolC activity in gut microbes

Statins have been widely studied for their potential as non-traditional antibiotics, with simvastatin garnering particular attention for its activity against multidrug resistant pathogens such as *Staphylococcus aureus*⁵⁸. Simvastatin alters the composition of gut microbiome in patients, but the mechanism driving this microbial shift is not understood²⁵. In our transcriptomic screening, we found that simvastatin strongly upregulated *acrAB-tolC* genes across multiple *Bacteroidales* strains, while atorvastatin significantly upregulated *acrAB-tolC* genes only in *P. distasonis* (Fig. 3d). Interestingly, these transcriptional profiles correlated with strong and modest toxicities exhibited in our growth screens by simvastatin and atorvastatin, respectively (Fig. 1b), motivating further exploration into the role of AcrAB-TolC in the interplay between gut microbes and antimicrobial compounds.

In *Bacteroides* species, the AcrAB-TolC efflux pump ameliorates toxicity of antibiotics and common dietary metabolites such as retinol (vitamin A)⁵⁷. We thus hypothesized that drugs altering AcrAB-TolC expression in *Bacteroidales* species could result in targeted changes in the toxicity of other compounds. Using *P. distasonis*, we first determined the MIC of retinol (>24 µg/mL) and several common antibiotics with different mechanisms of action whose resistance is mediated by AcrAB-TolC⁵⁶ (Supplementary Table 10). In the presence of simvastatin, the MICs of several of these compounds were significantly shifted, with retinol showing the most pronounced effect (>2-fold decrease, Supplementary Fig. 9). We then exposed four *Bacteroidales* strains (*P. distasonis* H1, *P. dorei* H1, *P. vulgatus* H1, *P. vulgatus* ATCC 8482) to retinol in the presence or absence of statins and additional drugs (sertraline, trazodone, amlodipine) observed to upregulate the *acrAB-tolC* operon (Fig. 4a; Supplementary Fig. 10). As a negative control, we co-incubated retinol-exposed non-*Bacteroidales* strains (*E. coli*, *A. rectalis*, *D. longicatena*) with simvastatin (Supplementary Fig. 11). At 20 µM, simvastatin enhanced the sensitivity to retinol in all *Bacteroidales* strains, with the strongest shift seen in *P. distasonis* and *P. vulgatus* (4-fold reduction in MIC, Fig. 4a). In non-*Bacteroidales* strains (*E. coli*, *D. longicatena*, *A. rectalis*), retinol MICs were not significantly altered by simvastatin co-incubation (Supplementary Fig. 11). Notably, we observed a modest shift approaching significance in simvastatin-treated *A. rectalis*, which we attribute to combined global toxicity burdens of simvastatin and retinol, unrelated to the AcrAB-TolC pump. Sertraline modestly increased retinol sensitivity in all *Bacteroidales* strains, amlodipine showed similar effects in two of four strains (*P. vulgatus* H1, *P. dorei* H1), atorvastatin modestly decreased the MIC of retinol in *P. distasonis* only, and trazodone did not significantly influence MIC of retinol in any strains (Fig. 4a, Supplementary Fig. 10).

Deoxycholic acid (DCA) is a secondary bile acid whose toxicity is also modulated by AcrAB-TolC⁵⁷. We thus tested whether simvastatin enhanced DCA toxicity in *P. distasonis*. Simvastatin at 20 µM significantly limited *P. distasonis* growth when co-incubated with DCA (MIC = 64 µg/ml, 66% reduction) (Fig. 4b). Simvastatin did not lower the MIC of other secondary bile acids (i.e., hydroxydeoxycholic acid, ursodeoxycholic acid) whose toxicity is not mediated by AcrAB-TolC⁵⁷ (Supplementary Fig. 12). Importantly, the simvastatin-altered MICs of retinol and DCA each fall within estimated colon concentration ranges of these metabolites in the human gut^{57,59}.

Having established that simvastatin significantly upregulates AcrAB-TolC in *Bacteroidales* species, and that this exposure increases *Bacteroidales* sensitivity to retinol and DCA, we next sought to confirm that AcrAB-TolC upregulation directly increases sensitivity to dietary metabolites. In order to establish causality of AcrAB-TolC upregulation in increasing collateral sensitivity of *Bacteroidales* species to retinol, we engineered a *P. vulgatus* H1 isolate to overexpress different copies of AcrAB-TolC or a control cargo, and measured retinol MIC for engineered isolates exposed to simvastatin or DMSO (Fig. 4c, Methods). As compared to plasmid overexpression of a cargo control, overexpression of either copy of AcrAB-TolC increased collateral sensitivity to retinol, establishing that efflux pump overexpression directly increases collateral sensitivity to vitamin A. Notably, while minimal toxicity was associated with plasmid overexpression in the control *P. vulgatus* strain, *acrAB-tolC* expression also increased toxicity of simvastatin at 20 μ M concentrations, as exhibited by *P. vulgatus* growth at retinol concentrations of zero. Further, overexpression of *acrAB-tolC* copy 2 caused greater enhancement of retinol and simvastatin toxicity in *P. vulgatus* as compared to copy 1, suggesting distinct efficacy levels of these genomic efflux pump copies. Taken together, our transcriptomic dataset revealed a statin-mediated interaction with the AcrAB-TolC efflux pump that could enhance the antimicrobial effects of common dietary and host metabolites *in vivo*, potentially accounting for the gut microbiota alterations seen in statin-treated patient populations²⁵.

Simvastatin is generally administered as a lactone prodrug, while atorvastatin is administered in the active compound form⁵⁸ (Fig. 4d). Given the role of lactone moieties in many antibiotics⁶⁰, we wondered whether the transcriptional regulation of the AcrAB-TolC efflux pump by simvastatin might be linked to the toxicity of its lactone moiety. To test whether the lactone ring in simvastatin induces toxicity, we incubated simvastatin-sensitive *P. distasonis* and *P. vulgatus* strains with the lactone prodrug (simvastatin), the non-lactone activated compound (tenivastatin), and atorvastatin (Fig. 4e). Interestingly, tenivastatin, which does not contain a lactone ring, did not exhibit toxicity against either tested strain. Notably, AcrAB-TolC preferentially binds to hydrophobic substrates (e.g., lipophilic lactone side chains)^{61,62}. To determine whether AcrAB-TolC modulation of bacterial inhibition by dietary metabolites depends on the presence of the toxic simvastatin lactone moiety, we exposed a *P. distasonis* strain to various concentrations of retinol in the presence or absence of 20 μ M simvastatin or tenivastatin (Fig. 4f). Tenivastatin did not lower the MIC of retinol, suggesting that the intact lactone ring of the unmetabolized prodrug simvastatin is necessary to enhance bacterial retinol sensitivity.

Next, to better understand the prevalence of AcrAB-TolC in the human gut microbiome, we assessed its frequency in 4,930 representative metagenome-assembled genomes (MAGs) sourced from healthy human microbiomes (Fig 5a, Methods)⁶³. 106 MAGs contained a complete AcrAB-TolC homolog (e $<10^{-5}$, coverage $>90\%$, identity $>40\%$), of which 59.4% were linked to the *Bacteroidaceae* family. The high prevalence of *AcrAB-TolC* in *Bacteroidaceae* suggests that *Bacteroidaceae*-dominated individuals may be particularly susceptible to simvastatin-mediated microbiota changes.

To explore the clinical relevance of simvastatin-induced upregulation of the *acrAB-tolC* operon, we next quantified the metagenomic abundance of this operon's homologs in stool

samples from the Body Mass Index Spectrum (BMIS) cohort²⁵ (Fig. 5b-d). Notably, the AcrAB-TolC pump was highly prevalent in fecal metagenomes of the BMIS cohort, with 91.6% of study participants showing >20% median relative abundance of AcrAB-TolC across treatment groups (Fig. 5b). Further, a significant decrease in relative abundance of the *acrAB-tolC* operon ($p_{adj} = 0.0102$) in the gut microbiome of patients receiving simvastatin was observed (Fig. 5b). In contrast, *acrAB-tolC* gene abundance was not changed in patients who received atorvastatin, fluvastatin, pravastatin, or rosuvastatin. Accordingly, simvastatin-treated patients also showed a significant depletion in *Bacteroides* species ($p = 0.0030$), as well as increases in *Alistipes* and unclassified *Firmicutes* (Fig. 5c). Moreover, *Bacteroides* and other bacteria containing a complete AcrAB-TolC homolog were significantly depleted in simvastatin-treated cohorts as compared to untreated controls ($p = 0.0013$), whereas bacteria missing this operon were not depleted ($p = 0.699$) (Fig. 5d). Notably, a relative abundance analysis for the separate gene components of the *acrAB-tolC* operon in statin-treated cohorts identified the most significant depletion ($p = 0.003$) in the *AcrB2* gene, which encodes a homotrimer docked to the intracellular bacterial membrane that binds to pump substrates (Supplementary Fig. 13)⁶¹.

Taken all together, we posit a potential model of statin-mediated depletion of gut microbes containing the AcrAB-TolC efflux pump (Supplementary Fig. 14). Under normal conditions, gut microbial residents containing AcrAB-TolC homologs (e.g., *Bacteroidales* species) utilize this pump to prevent periplasmic and cytoplasmic accumulation of metabolites, such as retinol and deoxycholic acid, to toxic levels. In the context of simvastatin treatment, *acrAB-tolC* is upregulated, leading to increased collateral sensitivity to dietary metabolites and reduced cell viability. Efflux pump upregulation leading to decreased bacterial viability has been observed in clinical cohorts⁶⁴, although the mechanism of this phenomenon has not been elucidated to date. Notably, the prototypical *acrAB-tolC* operon is regulated by the self-contained *acrR* repressor (Fig. 3d), which in *E. coli* is strongly upregulated under conditions of global stress⁶⁵. Thus, it is possible that by inducing AcrR expression, engineered AcrAB-TolC pump overexpression could indirectly impact co-regulation of global stress response and lead to reduced cell viability. Regardless, with simvastatin treatment, increased expression of AcrAB-TolC causes decreased viability of gut bacteria and consequential alterations in gut microbiota composition.

Strain differences in drug-mediated transcriptomic responses

Finally, we sought to explore how drug-microbe transcriptional responses differed among different strains in our panel (Fig. 6, Supplementary Fig. 15). First, we analyzed the DEGRs across all drugs by principal coordinates analysis (PCoA) to quantify similarities in global transcriptomic profiles of strains. Interestingly, we found that microbial responses to drugs clustered significantly at the family level (i.e., *Bacteroidaceae*, *Lachnospiraceae*), ($p = .003$ by PERMANOVA test) (Fig. 6a), suggesting that closely related bacteria may respond similarly to different drugs. However, a detailed comparison of conspecific strains revealed a more variable pattern of response. For example, while strains of *A. rectalis* (H1 vs. ATCC 33656) exhibited highly consistent drug responses, strains of *B. uniformis* (H1 vs. ATCC 8492) responded more heterogeneously to pharmaceuticals (Fig. 6a).

To further delineate the strain specificity of drug responses, we next quantified the average nucleotide similarity (ANI) between different *Bacteroidales* strain pairs, which we compared with the correlation of global transcriptomic response (DEGR values) between strains (Fig. 6b). We observed higher correlations ($R > 0.7$) in overall drug response between pairs with the greatest ANI values ($ANI > 0.95$), suggesting that the more similar the bacterial genome, the more similar the global transcriptomic response across drug conditions (Fig. 6b). In order to compare the transcriptomic responses of conspecific strains more closely, we next aligned the genomes for all conspecific strains (Methods). We observed high correlations ($R^2 > 0.79$) in expression of shared genes between all conspecific strain pairs, suggesting shared transcriptional responses between isolates (Supplementary Fig. 15).

We next sought to investigate strain-level drug response at the operon level. Remarkably, we identified two common types of transcriptional differences between conspecific strains: 1) absence of an operon in one isolate, and 2) differential regulation of a shared operon between isolates, with both differences possibly having functional impacts. For example, sertraline upregulated a mobile element containing Type IV secretion system machinery in *A. rectalis* H1 that was not present in *A. rectalis* ATCC 33656 (Fig. 6c). Similarly, sertraline and paroxetine upregulated BepE efflux machinery in *B. uniformis* H1 that was not present in ATCC 8492 (Fig. 6c). On the other hand, several drugs (sertraline, paroxetine, levothyroxine, simvastatin) downregulated a shared putative L-arabinose utilization operon in *A. rectalis* H1, but this same operon (98.31% average conservation in coding sequence) was not differentially expressed in *A. rectalis* 33656 (Fig. 6c). Conversely, these compounds downregulated a shared putative transketolase operon (99.89% average conservation in coding sequence) in *A. rectalis* 33656 only (Fig. 6c). Interestingly, in addition to differences in shared operon expression between isolates, we also observed instances of differential regulation of different gene copies by the same drug perturbation (Fig. 6c). For example, within *F. saccharivorans* DSMZ 26062, levothyroxine, sertraline, simvastatin, and paroxetine exposures triggered simultaneous up- and down-regulation of different copies of *araQ*, a permease protein associated with L-arabinose transport (99.25% average conservation in coding sequence; Fig. 6c). A high degree of strain-level functional diversity could explain the substantial microbiome compositional variation often observed in clinical drug studies that only rely on 16S taxonomic analysis rather than whole genome sequencing. Together, these results underline the importance of assessing bacterial drug responses at the strain level with genomic information, as well as extending traditional microbiota drug screens to multiple conspecific strains to capture the full intra-strain diversity of drug responses.

DISCUSSION

While numerous clinical studies suggest prevalent drug-microbiota interactions^{5,13,23,25}, genetic-level understanding of xenobiotic-induced microbiota shifts remains limited. In this study, we generated to our knowledge the largest transcriptome dataset for exploring gut microbiota-drug responses to common orally delivered drugs, totaling >400 bacterial-drug pairwise interactions. With this dataset, we uncovered that simvastatin-mediated upregulation of the AcrAB-TolC efflux pump generates collateral toxicity to dietary metabolites *ex vivo*. Using a clinical metagenomic dataset, we confirmed that AcrAB-

TolC-containing gut bacteria are depleted in patients taking simvastatin, suggesting that upregulation of *acrAB-tolC* under statin exposure increases cellular toxicity.

Beyond statins, our data established clinically relevant links between cardiovascular medications and SSRIs and the gut microbiome. Our *ex vivo* data and computational analysis of T2D patient data suggest the upregulation of tartrate metabolism in gut microbes exposed to metoprolol. This result motivates the need for further clinical studies to determine whether metoprolol tartrate places patients at higher risk for developing T2D and other metabolic disorders. The clinical dataset used in our analysis does not distinguish metoprolol tartrate versus metoprolol succinate, which are used short- or long-form treatment. As metoprolol tartrate exhibits a greater inter-individual variation in bioavailability⁴⁴, future work exploring the impact of microbiome metabolism on the *in vivo* bioavailability of metoprolol tartrate and other tartrate-conjugated pharmaceuticals is warranted. Separately, our findings provide the first evidence that drugs can modulate riboflavin production by gut bacteria. Mechanistic delineation of how pharmaceuticals induce or repress vitamin B2 production could enable the development of tools to promote microbial production of this essential vitamin⁵¹. As vitamin B2 depletions have been linked to depression and atherosclerosis^{52,53,55}, our data also motivate clinical studies of whether *rib*-modulating medications impact key vitamin reservoirs in the microbiomes of psychiatric and cardiovascular patients, and whether these interactions impact disease pathology.

From an ecological standpoint, shared transcriptional responses could provide mechanistic insights into how pharmaceuticals drive shifts in microbiome populations over time. Our pathway meta-analysis demonstrated that many drugs upregulate highly conserved bacterial multidrug efflux pumps. Efflux-associated pathways were distinct from resistance pathways upregulated by traditional antibiotics, suggesting novel mechanisms of drug-driven microbiota responses. Our results showing efflux-mediated collateral toxicity induced by simvastatin-retinol coinubation underline the importance of exploring the molecular efflux networks to identify drug-efflux pump interactions that can result in gut microbiota shifts. Further, recent data has linked chronic prescription drug use and polypharmacy with antimicrobial resistance in gut microbiota⁴. One work even linked the upregulation of efflux pumps by four antidepressants used in our study (sertraline, duloxetine, escitalopram, bupropion) to the promotion of antimicrobial resistance among gut community members⁶⁶. These data all suggest that chronic medication-induced increases in the activity of efflux pumps could contribute to higher rates of antimicrobial resistance among gut microbiota within patient populations.

Our study has several limitations. *Ex vivo* screens cannot capture the full environmental complexity that may exist between microbiota community members and the host *in vivo*, and transcriptomics does not directly probe host-mediated drug-microbiota interactions. While many of our observed inhibitory drug activities aligned with published clinical data^{5,25}, we detected neither growth nor transcriptional changes in gut bacteria exposed to metformin. The role of host-derived factors mediating metformin-induced microbiota shifts is well documented (i.e., secondary bile acids cause depletion of *Bacteroides* and enrichment of *Escherichia* species that trigger downstream regulation of the farnesoid receptor)⁶⁷. This and other instances of low transcriptomic signals generated in our study by drugs linked to

microbiota changes *in vivo* (e.g., omeprazole) could suggest missing host- or community-derived factors, motivating future *in vivo* studies that integrate these other factors (e.g., bile acids and dietary vitamins). While we leveraged published clinical microbiome data to further validate our *ex vivo* drug-microbe interaction results, our simvastatin findings could benefit from prospective clinical trials designed to dissect the impacts of simvastatin and disease status on gut microbiota dynamics, and to determine whether AcrAB-TolC is simply a biomarker or a functional mediator of simvastatin-associated gut microbiota shifts.

Altogether, this work has demonstrated the utility of high-throughput transcriptomics to delineate microbiota-drug interactions. We envision that this low-cost and scalable pipeline can be easily applied to any microbiota-treatment pairing including xenobiotic, prebiotic, and probiotic treatments. These efforts will lead to a greater mechanistic understanding of how different environmental exposures impact the gut microbiome that in turn can affect host health and response to medical interventions.

ONLINE METHODS

Materials and Culture Conditions

All bacteria used in this study have fully sequenced genomes, the information for which can be found in (Supplementary Table 3). Natural bacterial isolates used in this study were derived from a single fecal sample taken from a healthy individual for an unrelated study. Sex and gender of this individual, while reported in the unrelated study, were deemed irrelevant in this study and were not reported. This work was approved and conducted under Columbia University Medical Center Institutional Review Board protocol AAAR0753, and written informed consent was obtained from the subject. Additional conspecific strains of *A. rectalis*, *F. saccharivorans*, *B. uniformis*, *P. vulgatus*, and *B. fragilis*, as well as the *Eggerthella lenta* strain described in Ref¹⁵, were obtained from public strain catalogs. All publicly available strains used in this study were either purchased from the American Type Culture Collection (Manassas, VA) or the Leibniz Institute DSMZ-German Collection of Microorganisms and Cell Cultures GmbH. All monoclonal isolates were Sanger sequenced (Azenta Life Sciences) at the 16S-V4 region pre- and post-experimentation to confirm strain identity. Natural isolates used in this study are available from the corresponding author upon request.

For our drug panel, we selected 19 orally administered drugs from the top prescribed pharmaceuticals in 2017 according to the Agency for Healthcare Research and Quality (Supplementary Table 4)³¹. This list included the top eight most prescribed drugs, included lisinopril, atorvastatin, levothyroxine, metformin, amlodipine, metoprolol, omeprazole, and simvastatin. Additional neurotransmitter modulators were selected from the top 25 drugs prescribed, as follows: sertraline, fluoxetine, citalopram, escitalopram, paroxetine, duloxetine, venlafaxine, amitriptyline, bupropion, and trazodone. We finally included lenalidomide due to its large market cap³¹. All chemicals used in this study were purchased from Sigma-Aldrich (Burlington, MA), Thermo Scientific Chemicals (Waltham, MA), or Avantor (Phillipsburg, NJ) (Supplementary Tables 4, 9-10). Probes for rRNA depletions were purchased from Integrated DNA Technologies (Coralville, IA). Unless otherwise noted, bacterial cultures were grown in ½ diluted Gifu Anaerobic Medium Broth, modified

(mGAM, HyServe 05433) media prepared according to manufacturers' instructions. Prior to experimentation, all mGAM media was reduced for 24 hours under anaerobic conditions (5% H₂, 10% CO₂, 85% N₂) within a Coy Laboratory products anaerobic chamber. Chemical plates were prepared in 96-well format under aerobic sterile conditions and reduced for 3–6 hours prior to experimentation.

Bacterial Transcriptome Preparation and Extraction

For all transcriptomic experiments, bacterial cultures at exponential phase were added to 96- deep-well plates (Axygen P-DW-20-C) containing pre-reduced chemicals to reach a final concentration of 20 μ M (500 μ M for metformin). After 90 minutes of exposure in shaken media at 37°C, cultures were centrifuged, supernatant removed, and cell pellets were transferred to –80°C prior to bacterial RNA extraction.

Bacterial RNA was extracted using RNAsnap methods⁶⁸. Briefly, frozen bacterial pellets were suspended in 500 μ l RNAsnap mix (95% formamide, 18 mM ethylenediaminetetraacetic acid, 0.025% sodium dodecyl sulphate, 1% B-mercaptoethanol) before addition of ~200 μ l of 0.1mm Zirconia Silica beads (Biospec 11079101Z). Cells were then lysed by bead beating for 3 \times 2.5 minutes in a Biospec Mini Bead Beater (Biospec 1001) with 5-minute intervals and then subjected to centrifugation at 4,300 g for 5 minutes. The clean supernatant was then transferred to a new deep well plate and RNA was purified using a Zymo ZR-96 RNA Clean & Concentrator kit (Zymo R1080) per manufacturer's instructions.

RNA-seq Library Preparation and Sequencing

RNA-seq libraries were constructed following a modified RNAtag-seq protocol as detailed in Ref²⁴. Briefly, 400 ng of total RNA lysate was subjected to fragmentation in 2X FastAP buffer (ThermoFisher EF0651), genomic DNA removal (TURBO™ DNase, ThermoFisher AM2239), and dephosphorylation (FastAP, ThermoFisher EF0651). Fragmented RNA was purified using SeraPure SPRI bead cleanup⁶⁹ and ligated with barcoded first adapter ligation by T4 RNA ligase I (NEB M0437M). After pooling and purification with the Zymo RNA Clean and Concentrator-5 kit (Zymo R1015), we quantified barcoded RNA using a Qubit RNA HS Assay Kit (ThermoFisher Q32855) and then performed RNase H-based ribosomal RNA depletion on 400 ng of barcoded RNA sample using a 10:1 probe-to-RNA ratio, as previously outlined²⁴.

rRNA-depleted RNA was subjected to downstream library preparation following standard RNAtag-seq protocols²⁷, including reverse transcription (ThermoFisher 18090010) and second adapter ligation (NEB M0437M). Ligation products were further amplified with primers containing Illumina P5 and P7 adapters and sample indexes, and PCR reactions were stopped during exponential amplification. PCR products were subjected to gel electrophoresis on E-Gel™ EX Agarose Gels, 2% (ThermoFisher G402002) and expected DNA smears (300–600 bp) were excised and extracted using the Monarch™ DNA gel Extraction Kit (NEB T1020L). Resulting libraries were sequenced to a minimum of 4.9X (Supplementary Table 6). Sequences of all adapters and primers used in library preparation are provided in Ref²⁴.

RNA-seq Data Analyses

RNA libraries were analyzed for differential expression analysis as outlined in Ref²⁴, which lists all adapter and primer sequences used. Briefly, raw sequencing reads were demultiplexed using Sabre⁷⁰ and bcl2fastq⁷¹ prior to adapter removal with Cutadapt v2.1⁷², using parameters ‘-a file:[RNAseq adapter.fa] -u 5 –minimum-length 20 –max-n 0 -q 20’ to remove low-quality bases and adapters. To mitigate the effect of rRNA reads, we performed alignments against the 16S and 23S rRNAs of corresponding strains with Bowtie2⁷³, using the versions and parameters outlined in ²⁴. Genomes of natural isolates used for sequencing alignments were *de novo* assembled as described in²⁴. Genome assemblies for all publicly available isolates were downloaded from the NCBI database, with all accession numbers listed in (Supplementary Table 3). The number of reads uniquely mapped to each coding sequence was calculated using featureCounts v1.6.2⁷⁴ without restraint on strandness (-s 0), and the expression level of each CDS by transcripts per million (TPM) was quantified using an in-house script.

Finally, we used DESeq2⁷⁵ to perform differential expression analysis on the number of reads uniquely mapped to each coding sequence, calculating the FC of gene expression after perturbations. Differential gene expression was defined as >2 fold-change (FC) in gene expression relative to a vehicle control, with $p_{adj} < 0.05$, and average fragments per kilobase per million reads aligning to annotated open reading frame (FPKMO) > 0.10. P-values of differential expression were all adjusted by the Benjamini–Hochberg procedure in DESeq2 using default settings. Identified DEGs were used to identify drug-enriched modules and pathways using the Kyoto Encyclopedia of Genes and Genomes (KEGG) database⁷⁶. KEGG enrichment with $p_{adj} < 0.05$ and $e < 0.00001$ was considered statistically significant. All analyses were visualized in R⁷⁷.

Growth Assays

For all growth experiments, overnight bacterial cultures were back-diluted 1:100 before addition to 96-well plates containing 5–25 μ l of pre-reduced chemicals or bile acids to reach 2, 20, or 100 μ M concentrations in 1 ml of solution (all concentrations for bacterial-drug pairings listed in Supplementary Fig. 2). As an exception, higher concentrations of 50, 500 and 2500 μ M were used for metformin (Methods, Supplementary Fig. 2), which has much higher predicted drug concentrations in the intestinal tract⁵. Further, *A. shahii* was not included in growth experiments it exhibits characteristically poor growth in liquid that prevents optical density measurements⁷⁸. Cultures were then incubated at 37°C in shaken media for 24 hours. For 24-hour temporal growth screens, 190 μ l of culture was harvested at 6, 10, and 24 hours for measurement of optical density at 600 nm (OD⁶⁰⁰) using an Epoch2 Microplate Spectrophotometer (Agilent Technologies). For all MIC tests, cultures were harvested for visual inspection and OD⁶⁰⁰ measurement at 24 hours only. Growth inhibition was defined in all growth experiments as relative growth depletion >30%, with false discovery rate (FDR)-adjusted p value (p_{adj}) < 0.05. To determine statistical differences in relative growth between conditions, two-sided independent t-tests with Benjamini & Hochberg correction were performed in R to determine FDR-adjusted p-values unless otherwise stated.

Analysis of Public Datasets

To identify species harboring the *acrAB-toIC* operon, we generated an amino acid reference from the *P. vulgatus* *acrAB-toIC* operon detailed in⁵⁷. We then performed a homolog search for this reference operon in a public dataset of 4930 representative metagenome-assembled genomes (MAGs) characterized in Ref⁶³. Briefly, we annotated all putative protein sequences in the MAG dataset using Prokka⁷⁹ before performing a homolog search with blastP⁸⁰. Gene targets with an e-value < 10⁻⁵, coverage > 90% and identity > 40% were considered hits. We then estimated abundances of all species containing the *acrAB-toIC* operon using metadata from Ref⁶³. All associated p-values were calculated by two-tailed independent t-test in R.

To examine whether metoprolol administration could be linked to the upregulation of the *ttd* operon *in vivo*, raw amplicon sequencing data from a public dataset (n=145) were downloaded from Sequence Read Archive (SRA) under accession code ERP002469. Single-ended raw reads were processed by Cutadapt v2.1⁷² with the following parameters “--minimum-length 24 -u 10 --trim-n -q 15” to remove low-quality bases and Illumina adapters. Reads passing quality filtering were then aligned against our *ttd* operon reference by Bowtie2 v2.3.4⁷³ in --very-sensitive mode. Read counts per gene were normalized by gene length and sequencing depth (i.e., reads per kilobase per million mapped reads) for expression-level quantification. All associated p-values were calculated using the Mann-Whitney test in R.

To examine whether simvastatin-modulated microbiota shifts could be linked to *acrAB-toIC* operon prevalence *in vivo*, raw amplicon sequencing data from the cross-sectional Meta-Cardis Body Mass Index Spectrum (BMIS) cohort (n = 888) were downloaded from the EMBL-EBI European Nucleotide Archive (ENA) under accession number PRJEB37249. Single-ended raw reads were processed by Cutadapt v2.1⁷² with the following parameters “--minimum-length 24 -u 10 --trim-n -q 15” to remove low-quality bases and Illumina adapters. Reads passing quality filtering were then aligned against our *acrAB-toIC* operon reference by Bowtie2 v2.3.4⁷³ in --very-sensitive mode. Read counts per gene were normalized by gene length and sequencing depth (i.e., reads per kilobase per million mapped reads) for expression level quantification. All associated p-values were calculated by two-tailed independent t-test in R.

AcrAB-ToIC Engineering Studies

All *Bacteroides* expression vectors were generated using Gibson assembly (NEBuilder 2x HiFi DNA assembly master mix), and polymerase chain reaction (PCR) fragments for cloning were generated using Q5 DNA Polymerase (NEB). We first generated two PCR fragments from a plasmid designed and constructed in our laboratory containing a constitutive *Bacteroidales* promoters described in Ref⁸¹ (additional features of this custom vector backbone are described in a separate manuscript currently under consideration) to drive expression of the AcrAB-ToIC gene copies. We then cloned AcrAB-ToIC copy 1 (primers TCTCGTCAAACAATATAAATAATATAAACATGAAAATGACAGTAAATAGTATGAA ATGT and

AGAAGGGCACCAATAACTGCCTTAAAAAATTAATTATTTCACGTCCACCGC) and copy 2 (primers TCTCGTCAAACAAATATAAATAATATAAACATGAAATTTTATTGCAAACCTACGT and AGAAGGGCACCAATAACTGCCTTAAAAAATTATTCTTTTTTGCCTTTGGTCATC) from the *P. vulgatus* H1 genome using PCR. A 3 fragment Gibson assembly was incubated at 50 °C for 1 hour to generate our plasmid construct. As a control, we cloned a tetracycline (Tet) resistance gene (described in Ref⁸²) into our plasmid construct in place of AcrAB-TolC cargo. Finally, AcrAB-TolC-containing plasmids (or Tet plasmid controls) were transformed into chemically competent NEB turbo cells. Transformed colonies were screened by PCR for the correct insert size length and whole plasmids were sequenced on an Illumina Nextseq 500/550 platform or using Plasmidsaurus (Eugene, OR). Vector constructs with the correct payload were used in subsequent conjugation experiments.

Before conjugation, donor strains harboring conjugative *Bacteroides* expression vectors were grown from a single colony in 5 ml of LB-Lennox media (BD) supplemented with 50 µg ml⁻¹ of carbenicillin and 50 µM DAP at 37 °C overnight (~10–16 h). We prepared donor and recipient *P. vulgatus* H1 cells and carried out conjugations as previously described in Ref⁸³ under anaerobic conditions. Transconjugant colonies were Sanger sequenced at the 16Sv4 region to confirm strain identity, and stable plasmid maintenance was confirmed by colony PCR using the primers listed above. Positive *P. vulgatus* transconjugants were then picked into 5 mL ½ mGAM supplemented with 20 µg/ml erythromycin and grown overnight. These strains were banked in glycerol stocks (25% glycerol final concentration) and stored at –80 °C. Subsequent growth curve experiments were done using overnight cultures grown from these glycerol stocks in ½ mGAM.

Conspecific Strain Gene Mapping

To compare the transcriptomic response for strains of the same species, we performed gene mapping for five pairs of conspecific strains used in this study. Briefly, all protein sequences of the strains were first annotated using Prokka⁷⁹. Protein alignment was then performed for the protein sequences of conspecific strains by blastP⁸⁰ using the parameters “-max_target_seqs 20 -evalue 0.001”. Hits with identity > 0.75 and coverage > 0.75 were considered as mapped genes for conspecific strains.

Statistics and Reproducibility

For all isolates generated in this study, individual of origins for isolated gut strains were assigned based on the defined identity of original feces (Supplementary Table 2), for which covariate analysis is not applicable. The specific number of bacterial strains used in this study (19) was chosen to allow for inclusion of major bacterial phyla within an individual donor microbiome, with replicates included as described in Methods to allow for statistical significance calculations. For clinical datasets analyzed, cohort assignment for individuals was taken from the metadata of the original study. Blinding was not possible during experiments as we were comparing transcriptional responses of different bacterial isolates to different drug conditions. Transcriptomic and growth processing within species was blinded as different drug conditions were processed together using pooled methods.

Data exclusion was based on sequencing coverage or genome quality to remove technical artifacts as described in the Methods section. The sample sizes in this study are either number of bacterial strains tested (with replicates, see below), or number of experimental or control cohort individuals taken from a publicly available dataset (for which sample size calculations were already performed). All sample sizes are listed in figure legends and methods sections where applicable. All in vitro assays on bacterial strains were performed with multiple (2–4) technical replicates, as noted in the methods section and figure legends where applicable, in order to confirm replicability and enable statistical significance calculations. All analyses of associated data were performed with the same parameters and criteria described in Methods section above. Data distribution was assumed to be normal, but this was not formally tested.

Supplementary Material

Refer to Web version on PubMed Central for supplementary material.

ACKNOWLEDGEMENTS

We thank members of the Wang laboratory for advice and comments on the manuscript. H.H.W. acknowledges relevant funding support from the NSF (MCB-2025515), NIH (2R01AI132403, 1R01DK118044, 1R01CA272898, 1R01EB031935, 1R21AI146817), ONR (N00014-18-1-2237, N00014-17-1-2353), Burroughs Wellcome Fund (1016691), Irma T. Hirschl Trust, and Schaefer Research Award. D.R. acknowledges relevant funding support from the Columbia Medical Scientist Training Program. R.U.S. was supported by a Fannie and John Hertz Foundation Fellowship and an NSF Graduate Research Fellowship (DGE-1644869). D.R.G. was supported by the Burroughs Wellcome Fund Postdoctoral Diversity Enrichment Program.

DATA AVAILABILITY

All sequencing data generated in this study have been submitted to the NCBI BioProject database (<http://www.ncbi.nlm.nih.gov/bioproject/>) under accession number PRJNA925551.

REFERENCES

1. IQVIA Institute. Global Medicine Spending and Usage Trends: Outlook to 2025. Published online 2021.
2. National Center for Health Statistics. Health, United States 2019. Published online 2019. Accessed October 14, 2022. <https://www.cdc.gov/nchs/hus/contents2019.htm#Table-039>
3. Sonnenburg JL, Sonnenburg ED. Vulnerability of the industrialized microbiota. *Science*. 2019;366(6464). doi:10.1126/SCIENCE.AAW9255/ASSET/698B3EE4-7BB6-4B68-9600-299710FA3189/ASSETS/GRAPHIC/366_AAW9255_FA.JPEG
4. Nagata N, Nishijima S, Miyoshi-Akiyama T, et al. Population-level Metagenomics Uncovers Distinct Effects of Multiple Medications on the Human Gut Microbiome. *Gastroenterology*. 2022;163(4):1038–1052. doi:10.1053/j.gastro.2022.06.070 [PubMed: 35788347]
5. Maier L, Pruteanu M, Kuhn M, et al. Extensive impact of non-antibiotic drugs on human gut bacteria. *Nature*. 2018;555(7698):623–628. doi:10.1038/nature25979 [PubMed: 29555994]
6. Jackson MA, Goodrich JK, Maxan ME, et al. Proton pump inhibitors alter the composition of the gut microbiota. *Gut* 2016;65(5):749–756. doi:10.1136/GUTJNL-2015-310861 [PubMed: 26719299]
7. National Center for Health Statistics. National Ambulatory Medical Care Survey: 2018 National Summary Tables. Published online 2018.
8. Singh R, Chandrashekarappa S, Bodduluri SR, et al. Enhancement of the gut barrier integrity by a microbial metabolite through the Nrf2 pathway. *Nat Commun* 2019 10. 2019;10(1):1–18. doi:10.1038/s41467-018-07859-7 [PubMed: 30602773]

9. Roager HM, Hansen LBS, Bahl MI, et al. Colonic transit time is related to bacterial metabolism and mucosal turnover in the gut. *Nat Microbiol* 2016 19. 2016;1(9):1–9. doi:10.1038/nmicrobiol.2016.93
10. Wexler AG, Schofield WB, Degnan PH, Folta-Stogniew E, Barry NA, Goodman AL. Human gut bacteroides capture vitamin B12 via cell surface-exposed lipoproteins. *eLife*. 2018;7. doi:10.7554/ELIFE.37138
11. Gopalakrishnan V, Helmink BA, Spencer CN, Reuben A, Wargo JA. The Influence of the Gut Microbiome on Cancer, Immunity, and Cancer Immunotherapy. *Cancer Cell*. 2018;33(4):570–580. doi:10.1016/j.ccell.2018.03.015 [PubMed: 29634945]
12. Porras AM, Zhou H, Shi Q, et al. Inflammatory Bowel Disease-Associated Gut Commensals Degrade Components of the Extracellular Matrix. *mBio* 2022;13(6):e02201–22. doi:10.1128/mbio.02201-22 [PubMed: 36445085]
13. Gopalakrishnan V, Spencer CN, Nezi L, et al. Gut microbiome modulates response to anti-PD-1 immunotherapy in melanoma patients. *Science*. 2018;359(6371):97–103. doi:10.1126/science.aan4236 [PubMed: 29097493]
14. Khoruts A, Sadowsky MJ. Understanding the mechanisms of faecal microbiota transplantation. *Nat Rev Gastroenterol Hepatol* 2016;13(9):508–516. doi:10.1038/NGASTRO.2016.98 [PubMed: 27329806]
15. Haiser HJ, Gootenberg DB, Chatman K, Sirasani G, Balskus EP, Turnbaugh PJ. Predicting and manipulating cardiac drug inactivation by the human gut bacterium *eggerthella lenta*. *Science*. 2013;341(6143):295–298. doi:10.1126/science.1235872 [PubMed: 23869020]
16. Heinken A, Hertel J, Acharya G, et al. Genome-scale metabolic reconstruction of 7,302 human microorganisms for personalized medicine. *Nat Biotechnol* Published online January 19, 2023:1–12. doi:10.1038/s41587-022-01628-0 [PubMed: 36653493]
17. Zimmermann M, Zimmermann-Kogadeeva M, Wegmann R, Goodman AL. Separating host and microbiome contributions to drug pharmacokinetics and toxicity. *Science*. 2019;363(6427). doi:10.1126/science.aat9931
18. T K, H T, H M, et al. Involvement of beta-glucuronidase in intestinal microflora in the intestinal toxicity of the antitumor camptothecin derivative irinotecan hydrochloride (CPT-11) in rats. *Cancer Res* 1996;56(16):3752–3757. [PubMed: 8706020]
19. Klünemann M, Andrejev S, Blasche S, et al. Bioaccumulation of therapeutic drugs by human gut bacteria. *Nat* 2021 5977877. 2021;597(7877):533–538. doi:10.1038/s41586-021-03891-8
20. Zhang Y, Thompson KN, Branck T, et al. Metatranscriptomics for the Human Microbiome and Microbial Community Functional Profiling. <https://doi.org/10.1146/annurev-biodatasci-031121-103035>. 2021;4(1):279–311. doi:10.1146/ANNUREV-BIODATASCI-031121-103035
21. Lloréns-Rico V, Simcock JA, Huys GRB, Raes J. Single-cell approaches in human microbiome research. *Cell*. 2022;185(15):2725–2738. doi:10.1016/j.cell.2022.06.040 [PubMed: 35868276]
22. Spanogiannopoulos P, Kyaw TS, Guthrie BGH, et al. Host and gut bacteria share metabolic pathways for anti-cancer drug metabolism. *Nat Microbiol* 2022;7(10):1605–1620. doi:10.1038/s41564-022-01226-5 [PubMed: 36138165]
23. Rekdal VM, Bess EN, Bisanz JE, Turnbaugh PJ, Balskus EP. Discovery and inhibition of an interspecies gut bacterial pathway for Levodopa metabolism. *Science*. 2019;364(6445). doi:10.1126/science.aau6323
24. Huang Y, Sheth RU, Kaufman A, Wang HH. Scalable and cost-effective ribonuclease-based rRNA depletion for transcriptomics. *Nucleic Acids Res* 2020;48(4):E20. doi:10.1093/nar/gkz1169 [PubMed: 31879761]
25. Vieira-Silva S, Falony G, Belda E, et al. Statin therapy is associated with lower prevalence of gut microbiota dysbiosis. *Nat* 2020 5817808. 2020;581(7808):310–315. doi:10.1038/s41586-020-2269-x
26. Fuentes AV, Pineda MD, Venkata KCN. Comprehension of Top 200 Prescribed Drugs in the US as a Resource for Pharmacy Teaching, Training and Practice. *Pharm J Pharm Educ Pract* 2018;6(2):43. doi:10.3390/PHARMACY6020043

27. Shishkin AA, Giannoukos G, Kucukural A, et al. Simultaneous generation of many RNA-seq libraries in a single reaction. *Nat Methods* 2015 124. 2015;12(4):323–325. doi:10.1038/nmeth.3313 [PubMed: 25730492]
28. Turnbaugh PJ, Ley RE, Hamady M, Fraser-Liggett CM, Knight R, Gordon JI. The Human Microbiome Project. *Nature*. 2007;449(7164):804–810. doi:10.1038/nature06244 [PubMed: 17943116]
29. Derrien M, Turroni F, Ventura M, van Sinderen D. Insights into endogenous Bifidobacterium species in the human gut microbiota during adulthood. *Trends Microbiol* 2022;30(10):940–947. doi:10.1016/J.TIM.2022.04.004 [PubMed: 35577716]
30. Martinson JNV, Walk ST. Escherichia coli residency in the gut of healthy human adults. *EcoSal Plus*. 2020;9(1). doi:10.1128/ECOSALPLUS.ESP-0003-2020
31. Kane SP. The Top 300 of 2017. *ClinCalc Drugstats Database*. Published online 2021:10.
32. Goh EB, Yim G, Tsui W, McClure JA, Surette MG, Davies J. Transcriptional modulation of bacterial gene expression by subinhibitory concentrations of antibiotics. *Proc Natl Acad Sci U S A*. 2002;99(26):17025–17030. doi:10.1073/PNAS.252607699/ASSET/AC6FCBF7-AB76-4DD2-9DC3-CA3C136B2F28/ASSETS/GRAPHIC/PQ2526076006.JPEG [PubMed: 12482953]
33. Gibson B, Wilson DJ, Feil E, Eyre-Walker A. The distribution of bacterial doubling times in the wild. *Proc R Soc B Biol Sci* 2018;285(1880):20180789. doi:10.1098/rspb.2018.0789
34. Zhu Z, Surujon D, Ortiz-Marquez JC, et al. Entropy of a bacterial stress response is a generalizable predictor for fitness and antibiotic sensitivity. *Nat Commun* 2020 111. 2020;11(1):1–15. doi:10.1038/s41467-020-18134-z [PubMed: 31911652]
35. Vicente M, Chater KF, De Lorenzo V. Bacterial transcription factors involved in global regulation. *Mol Microbiol* 1999;33(1):8–17. doi:10.1046/J.1365-2958.1999.01445.X [PubMed: 10411719]
36. Cayres LC de F, de Salis LVV, Rodrigues GSP, et al. Detection of Alterations in the Gut Microbiota and Intestinal Permeability in Patients With Hashimoto Thyroiditis. *Front Immunol* 2021;12:453. doi:10.3389/FIMMU.2021.579140/BIBTEX
37. Bajaj JS, Sikaroodi M, Fagan A, et al. Microbiome and Host Interactions: Posttraumatic stress disorder is associated with altered gut microbiota that modulates cognitive performance in veterans with cirrhosis. *Am J Physiol - Gastrointest Liver Physiol* 2019;317(5):G661. doi:10.1152/AJPGI.00194.2019 [PubMed: 31460790]
38. Poole K Efflux-mediated multiresistance in Gram-negative bacteria. *Clin Microbiol Infect* 2004;10(1):12–26. doi:10.1111/j.1469-0691.2004.00763.x
39. Du D, Wang-Kan X, Neuberger A, et al. Multidrug efflux pumps: structure, function and regulation. *Nat Rev Microbiol* 2018;16(9):523–539. doi:10.1038/s41579-018-0048-6 [PubMed: 30002505]
40. Sun J, Deng Z, Yan A. Bacterial multidrug efflux pumps: Mechanisms, physiology and pharmacological exploitations. *Biochem Biophys Res Commun* 2014;453(2):254–267. doi:10.1016/j.bbrc.2014.05.090 [PubMed: 24878531]
41. Bryan LE, Kowand SK, Van Den Elzen HM. Mechanism of Aminoglycoside Antibiotic Resistance in Anaerobic Bacteria: Clostridium perfringens and Bacteroides fragilis. *Antimicrob Agents Chemother*. 1979;15(1):7–13. [PubMed: 218500]
42. Zimmermann M, Zimmermann-Kogadeeva M, Wegmann R, Goodman AL. Mapping human microbiome drug metabolism by gut bacteria and their genes. *Nature*. 2019;570(7762):462–467. doi:10.1038/s41586-019-1291-3 [PubMed: 31158845]
43. Morris J, Dunham A. Metoprolol. *XPharm Compr Pharmacol Ref* Published online July 11, 2022:1–7. doi:10.1016/B978-008055232-3.62174-9
44. Sandberg A, Blomqvist I, Jonsson UE, Lundborg P. Pharmacokinetic and pharmacodynamic properties of a new controlled-release formulation of metoprolol: A comparison with conventional tablets. *Eur J Clin Pharmacol* 1988;33(1):S9–S14. doi:10.1007/BF00578406 [PubMed: 3371395]
45. Kohn LD, Jakoby WB. Tartaric Acid Metabolism III. THE FORMATION OF GLYCERIC ACID. *J Biol Chem* 1968;243(10):2465–2471. doi:10.1016/S0021-9258(18)93398-3 [PubMed: 4297259]

46. Sobiecka A, Synoradzki L, Hajmowicz H, Zawada K. Tartaric Acid and its Derivatives. Part 17. Synthesis and Applications of Tartrates. *Org Prep Proced Int* 2017;49(1):1–27. doi:10.1080/00304948.2017.1260392
47. Proffitt C, Bidkhorji G, Lee S, et al. Genome-scale metabolic modelling of the human gut microbiome reveals changes in the glyoxylate and dicarboxylate metabolism in metabolic disorders. *iScience*. 2022;25(7):104513. doi:10.1016/j.ISCI.2022.104513 [PubMed: 35754734]
48. Cai L, Wu H, Li D, Zhou K, Zou F. Type 2 Diabetes Biomarkers of Human Gut Microbiota Selected via Iterative Sure Independent Screening Method. *PLoS One*. 2015;10(10):e0140827. doi:10.1371/journal.pone.0140827 [PubMed: 26479726]
49. Fuchs FD, Whelton PK. High Blood Pressure and Cardiovascular Disease. *Hypertension*. Published online 2020:285–292. doi:10.1161/HYPERTENSIONAHA.119.14240 [PubMed: 31865786]
50. Yoshii K, Hosomi K, Sawane K, Kunisawa J. Metabolism of dietary and microbial vitamin B family in the regulation of host immunity. *Front Nutr* 2019;6:48. doi:10.3389/FNUT.2019.00048/BIBTEX [PubMed: 31058161]
51. Averianova LA, Balabanova LA, Son OM, Podvolotskaya AB, Tekutyeva LA. Production of Vitamin B2 (Riboflavin) by Microorganisms: An Overview. *Front Bioeng Biotechnol* 2020;8:1172. doi:10.3389/FBIOE.2020.570828/BIBTEX
52. Wu Y, Zhang L, Li S, Zhang D. Associations of dietary vitamin B1, vitamin B2, vitamin B6, and vitamin B12 with the risk of depression: a systematic review and meta-analysis. *Nutr Rev* 2022;80(3):351–366. doi:10.1093/NUTRIT/NUAB014 [PubMed: 33912967]
53. Rouhani P, Amoushahi M, Keshteli AH, et al. Dietary riboflavin intake in relation to psychological disorders in Iranian adults: an observational study. *Sci Rep* 2023;13:5152. doi:10.1038/s41598-023-32309-w [PubMed: 36991113]
54. García-Minguillán CJ, Fernández-Ballart JD, Ceruelo S, et al. Riboflavin status modifies the effects of methylenetetrahydrofolate reductase (MTHFR) and methionine synthase reductase (MTRR) polymorphisms on homocysteine. *Genes Nutr* 2014;9(6):1–11. doi:10.1007/S12263-014-0435-1/FIGURES/3
55. Gebbers JO. Atherosclerosis, cholesterol, nutrition, and statins – a critical review. *GMS Ger Med Sci* 2007;5:Doc04. [PubMed: 19675712]
56. Okusu H, Ma D, Nikaïdo H. AcrAB efflux pump plays a major role in the antibiotic resistance phenotype of *Escherichia coli* multiple-antibiotic-resistance (Mar) mutants. *J Bacteriol* 1996;178(1):306. doi:10.1128/JB.178.1.306-308.1996 [PubMed: 8550435]
57. Hibberd MC, Wu M, Rodionov DA, et al. The effects of micronutrient deficiencies on bacterial species from the human gut microbiota. *Sci Transl Med* 2017;9(390). doi:10.1126/SCITRANSLMED.AAL4069/SUPPL_FILE/AAL4069_TABLES_S1_TO_S16.ZIP
58. Ko HHT, Lareu RR, Dix BR, Hughes JD. Statins: Antimicrobial resistance breakers or makers? *PeerJ* 2017;2017(10). doi:10.7717/PEERJ.3952/SUPP-1
59. Keating N, Mroz MS, Scharl MM, et al. Physiological concentrations of bile acids down-regulate agonist induced secretion in colonic epithelial cells. *J Cell Mol Med* 2009;13(8b):2293. doi:10.1111/J.1582-4934.2009.00838.X [PubMed: 19583809]
60. Lenz KD, Klosterman KE, Mukundan H, Kubicek-Sutherland JZ. Macrolides: From Toxins to Therapeutics. *Toxins*. 2021;13(5). doi:10.3390/TOXINS13050347
61. Jang S AcrAB–TolC, a major efflux pump in Gram negative bacteria: toward understanding its operation mechanism. *BMB Rep* 2023;56(6):326–334. doi:10.5483/BMBRep.2023-0070 [PubMed: 37254571]
62. Nikaïdo H, Basina M, Nguyen V, Rosenberg EY. Multidrug efflux pump AcrAB of *Salmonella typhimurium* excretes only those beta-lactam antibiotics containing lipophilic side chains. *J Bacteriol* 1998;180(17):4686–4692. doi:10.1128/JB.180.17.4686-4692.1998 [PubMed: 9721312]
63. Pasolli E, Asnicar F, Manara S, et al. Extensive Unexplored Human Microbiome Diversity Revealed by Over 150,000 Genomes from Metagenomes Spanning Age, Geography, and Lifestyle. *Cell*. 2019;176(3):649–662.e20. doi:10.1016/J.CELL.2019.01.001 [PubMed: 30661755]

64. Imamovic L, Ellabaan MMH, Dantas Machado AM, et al. Drug-Driven Phenotypic Convergence Supports Rational Treatment Strategies of Chronic Infections. *Cell*. 2018;172(1):121–134.e14. doi:10.1016/j.cell.2017.12.012 [PubMed: 29307490]
65. Ma D, Alberti M, Lynch C, Nikaido H, Hearst JE. The local repressor AcrR plays a modulating role in the regulation of *acrAB* genes of *Escherichia coli* by global stress signals. *Mol Microbiol* 1996;19(1):101–112. doi:10.1046/j.1365-2958.1996.357881.x [PubMed: 8821940]
66. Wang Y, Yu Z, Ding P, et al. Antidepressants can induce mutation and enhance persistence toward multiple antibiotics. *Proc Natl Acad Sci* 2023;120(5):e2208344120. doi:10.1073/pnas.2208344120 [PubMed: 36689653]
67. Lien F, Berthier A, Bouchaert E, et al. Metformin interferes with bile acid homeostasis through AMPK-FXR crosstalk. *J Clin Invest* 2014;124(3):1037–1051. doi:10.1172/JCI68815 [PubMed: 24531544]

METHODS ONLY REFERENCES

68. Stead MB, Agrawal A, Bowden KE, et al. RNAsnap™: a rapid, quantitative and inexpensive, method for isolating total RNA from bacteria. *Nucleic Acids Res* 2012;40(20). doi:10.1093/NAR/GKS680
69. Rohland N, Reich D. Cost-effective, high-throughput DNA sequencing libraries for multiplexed target capture. *Genome Res* 2012;22(5):939–946. doi:10.1101/GR.128124.111 [PubMed: 22267522]
70. Sabre- Barcode Demultiplexing. Accessed September 26, 2022. <https://github.com/najoshi/sabre>
71. Illumina. bcl2fastq Conversion User Guide. Published online 2013.
72. Martin M Cutadapt removes adapter sequences from high-throughput sequencing reads. *EMBnet.journal*. 2011;17(1):10–12. doi:10.14806/EJ.17.1.200
73. Langmead B, Salzberg SL. Fast gapped-read alignment with Bowtie 2. *Nat Methods* 2012 94. 2012;9(4):357–359. doi:10.1038/nmeth.1923 [PubMed: 22388286]
74. Liao Y, Smyth GK, Shi W. FeatureCounts: An efficient general purpose program for assigning sequence reads to genomic features. *Bioinformatics*. 2014;30(7):923–930. doi:10.1093/bioinformatics/btt656 [PubMed: 24227677]
75. Love MI, Huber W, Anders S. Moderated estimation of fold change and dispersion for RNA-seq data with DESeq2. *Genome Biol* 2014 1512. 2014;15(12):1–21. doi:10.1186/S13059-014-0550-8
76. Kanehisa M, Goto S. KEGG: Kyoto Encyclopedia of Genes and Genomes. *Nucleic Acids Res* 2000;28(1):27–30. doi:10.1093/nar/28.1.27 [PubMed: 10592173]
77. Andy Bunn MK. A language and environment for statistical computing. *R Found Stat Comput* 2017;10(1):11–18.
78. Parker BJ, Wearsch PA, Veloo ACM, Rodriguez-Palacios A. The Genus *Alistipes*: Gut Bacteria With Emerging Implications to Inflammation, Cancer, and Mental Health. *Front Immunol* 2020;11. Accessed January 15, 2023. <https://www.frontiersin.org/articles/10.3389/fimmu.2020.00906> [PubMed: 32082309]
79. Seemann T Prokka: rapid prokaryotic genome annotation. *Bioinformatics*. 2014;30(14):2068–2069. doi:10.1093/BIOINFORMATICS/BTU153 [PubMed: 24642063]
80. Altschul SF, Gish W, Miller W, Myers EW, Lipman DJ. Basic local alignment search tool. *J Mol Biol* 1990;215(3):403–410. doi:10.1016/S0022-2836(05)80360-2 [PubMed: 2231712]
81. Mimee M, Tucker AC, Voigt CA, Lu TK. Programming a Human Commensal Bacterium, *Bacteroides thetaiotaomicron*, to Sense and Respond to Stimuli in the Murine Gut Microbiota HHS Public Access. *Cell Syst* July. 2015;29(11):62–71. doi:10.1016/j.cels.2015.06.001
82. Jeters RT, Wang GR, Moon K, Shoemaker NB, Salyers AA. Tetracycline-Associated Transcriptional Regulation of Transfer Genes of the *Bacteroides* Conjugative Transposon CTnDOT. *J Bacteriol* 2009;191(20):6374–6382. doi:10.1128/jb.00739-09 [PubMed: 19700528]
83. Gelsinger DR, Vo PLH, Klompe SE, Ronda C, Wang H, Sternberg SH. Bacterial genome engineering using CRISPR RNA-guided transposases. Published online March 21, 2023:2023.03.18.533263. doi:10.1101/2023.03.18.533263

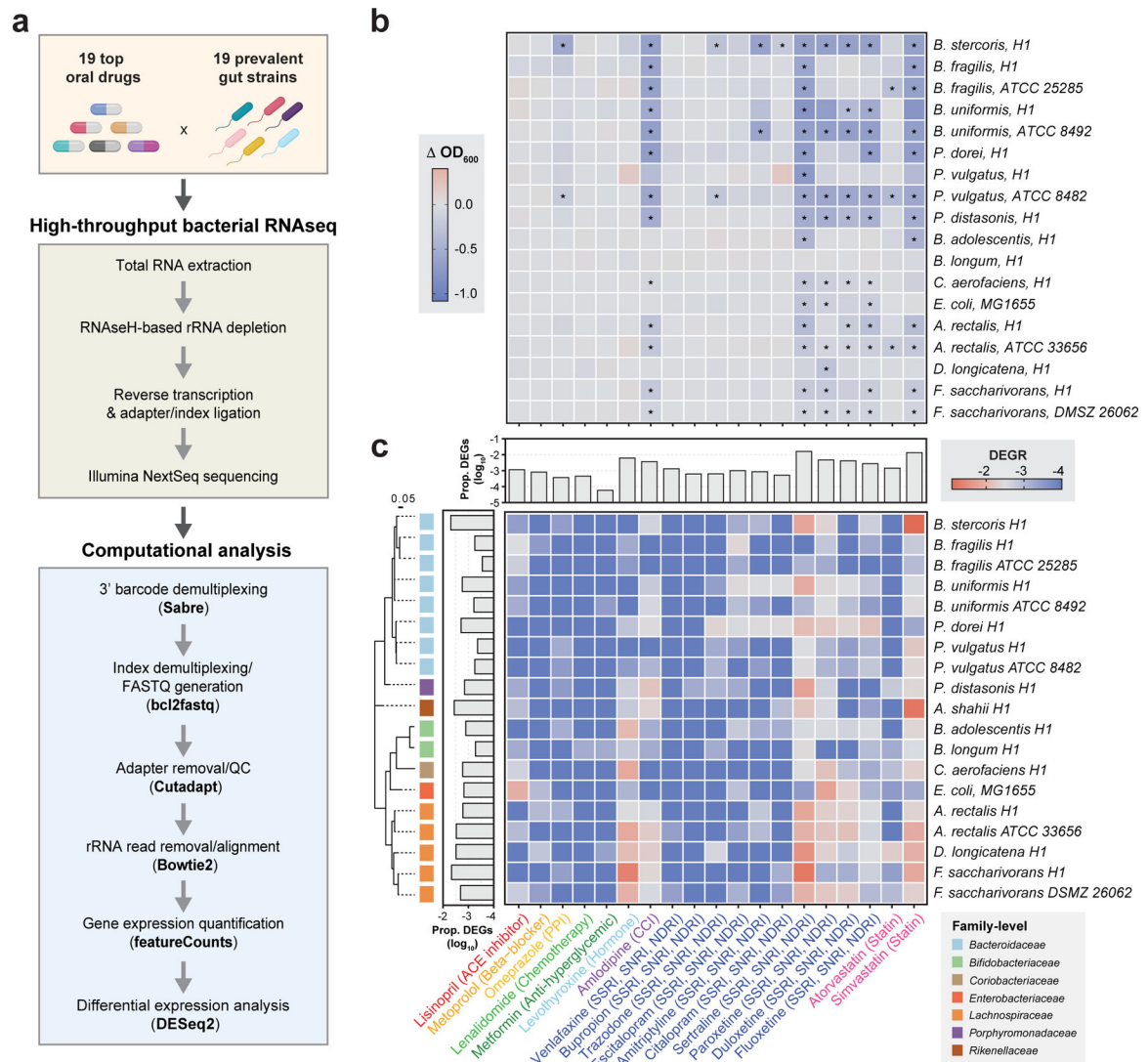


Figure 1. Top prescribed drugs elicit rich transcriptomic responses from prevalent gut bacterial species.

(a) Schematic of our high throughput transcriptomic pipeline for non-model gut microorganisms. (b) Heatmap color indicates delta in average optical density (OD) at 48 hours of bacterial strains grown in mGAM supplemented with different pharmaceuticals at 100 μM as compared to a same-volume solvent control ($n=3$ per condition). Drug condition is indicated on the x-axis and strain identity is indicated on the y-axis. Stars indicate >0.3 average absolute change in growth with $p_{\text{adj}} < 0.05$ (*), calculated by two-sided independent t-test with Benjamini & Hochberg correction (c) Bacterial strains were exposed to drugs ($n=2$ per condition) or vehicle controls ($n=4$ per condition) and differentially expressed genes ($p_{\text{adj}} < 0.05$, calculated as above) were identified. Heatmap color represents the \log_{10} value of the differentially expressed gene ratio (DEGR), defined as number of differentially expressed genes in a drug condition divided by total number of genes within a strain genome, with drug indicated on the x-axis (classes grouped by color) and strain identity indicated on the y-axis. Bar plot inserts show \log_{10} values of average DEGRs across strains

(top bar insert) or drugs (left bar insert). Maximum likelihood phylogenetic tree is shown on the left with bacterial family identity indicated by color in the figure legend.

Author Manuscript

Author Manuscript

Author Manuscript

Author Manuscript

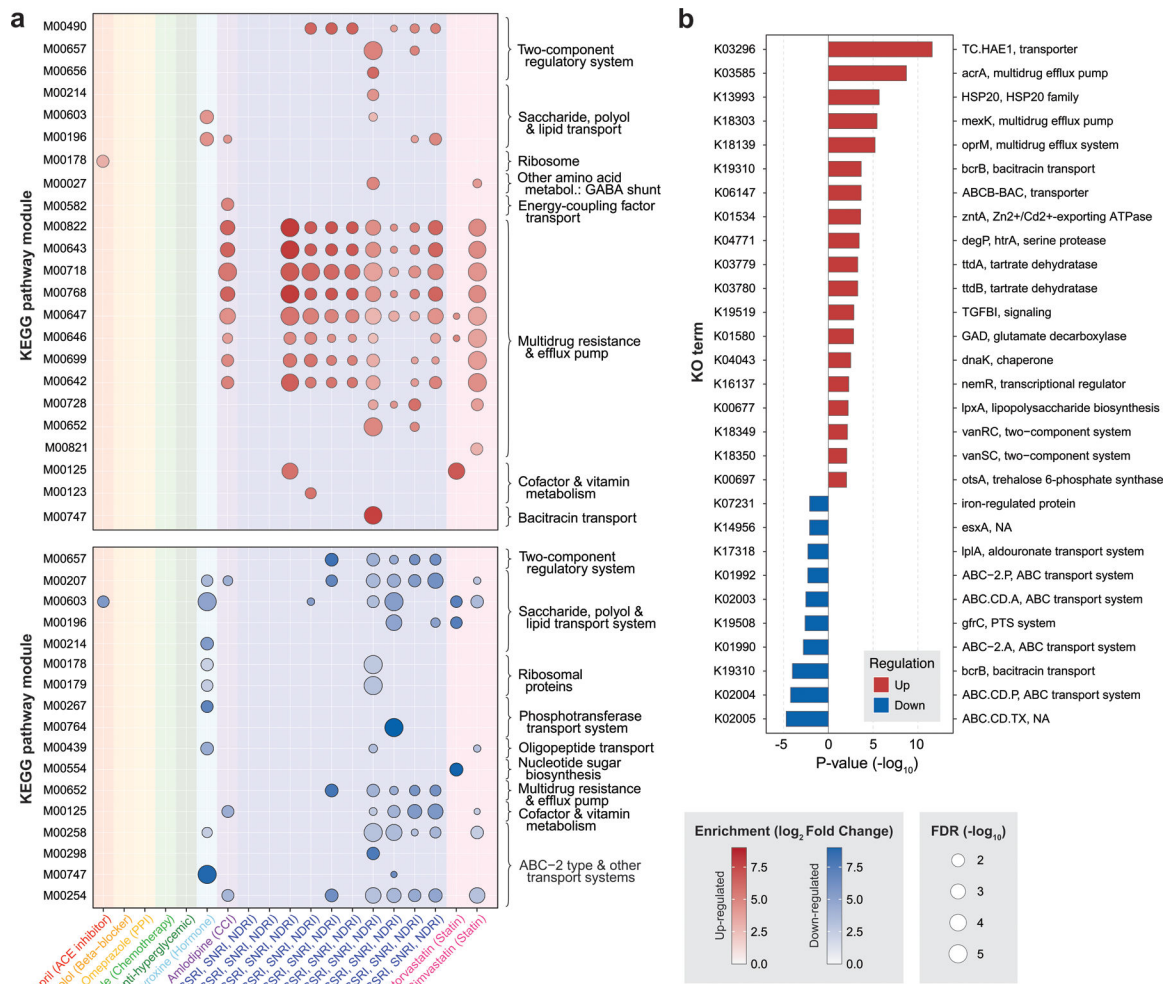


Figure 2. Pathway enrichment analysis reveals modulation of conserved efflux pathways by top pharmaceutical compounds.

(a) KEGG modules with significant enrichment ($p_{adj} < 0.05$ by two-sided independent t-test with Benjamini & Hochberg correction, $e\text{-value} < 10^{-5}$) based on pathway analysis of DEG datasets are shown. Drug condition is labeled on the x-axis and corresponds to background color of the bubble plot. IDs of KEGG modules with significant enrichment are labeled on the left y-axis, and KEGG pathway groups are labeled on the right y-axis. Bubble color indicates direction of regulation (red=up-regulation, blue=down-regulation), bubble intensity indicates $\log_2(FC)$ enrichment, and bubble size indicates level of significance ($-\log_{10}$ of p_{adj}). (b) Top 19 upregulated and top 10 downregulated functional orthologs within the DEG dataset across drugs, as annotated within the KEGG orthology (KO) database. Bar color indicates direction of transcriptional regulation as in (a). $-\log_{10}$ of p_{adj} (calculated as in (a)) is shown on the x-axis. K-number assigned by the KO database is labeled on the left y-axis, and putative ortholog function is labeled on the right y-axis.

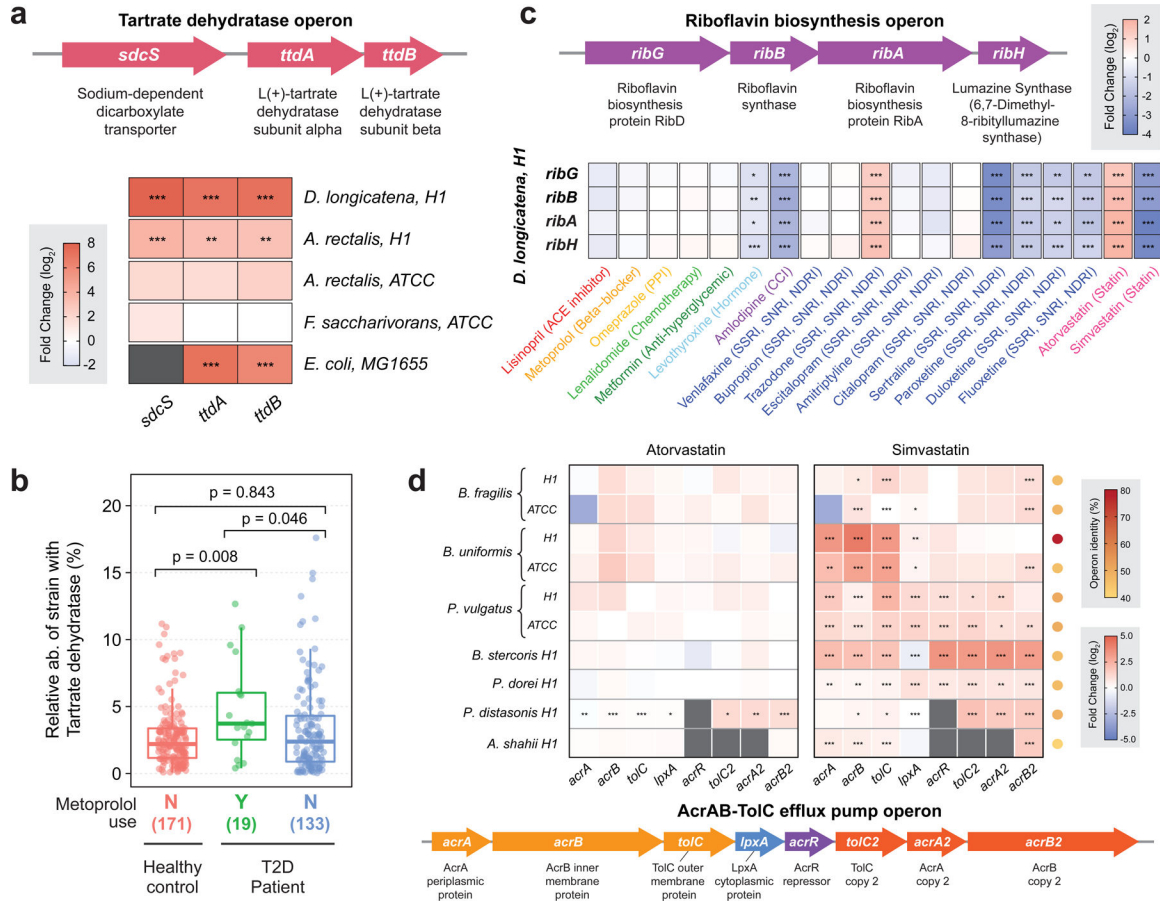


Figure 3. Top pharmaceutical compounds impact gut bacterial metabolism, vitamin production, and mitigation of toxic metabolites.

(a) Top schematic shows the components of the tartrate dehydratase (*ttd*) operon in *E. coli*. Genes within the operon are labeled on the x-axis, and isolates containing *ttd* analogs are labeled on the y-axis. Heatmap color indicates $\log_2(\text{FC})$ in transcripts per million (TPM) expression. Stars indicate $p_{\text{adj}} < 0.05$ (*), $p_{\text{adj}} < 0.01$ (**), $p_{\text{adj}} < 0.001$ (***) calculated by two-sided independent t-test with Benjamini & Hochberg correction. Gray panels indicate absence of a gene analog. (b) Relative abundance of bacterial isolates containing the *ttd* operon was calculated within a dataset of T2D patients⁴⁸ (n=323 total patients). The x-axis indicates patient cohort, grouped by healthy controls not taking metoprolol (red dots), T2D patients taking metoprolol (green dots), and T2D patients not taking metoprolol (blue dots). Relative abundance of isolates is shown on the y-axis. P-values calculated by two-sided independent t-test are annotated with brackets. (c) Top schematic shows the components of the riboflavin biosynthesis (*rib*) operon in *D. longicatena* H1. Drugs are labeled on the x-axis (grouped and colored by class), and gene components of the *rib* operon are labeled on the y-axis. Heatmap color indicates $\log_2(\text{FC})$ in TPM expression. Stars indicate significance as calculated and annotated in (a). (d) Regulation of *acrAB-toiC* within *Bacteroidales* isolates by atorvastatin (left panel) and simvastatin (right panel). Bottom schematic shows the components of the *acrAB-toiC* operon in *E. coli*. Genes within *acrAB-toiC* are labeled on the x-axis, and isolates containing AcrAB-TolC analogs are labeled on the y-axis.

Author Manuscript

Author Manuscript

Author Manuscript

Author Manuscript

Heatmap color indicates $\log_2(\text{FC})$ in TPM expression, as indicated by the bottom right red-to-blue color bar. Stars indicate significance as calculated and annotated in (a). Dots to the right of strain rows indicate percent operon identity as compared to the *P. vulgatus* AcrAB reference⁵⁷, as indicated by the top right red-to-yellow color bar.

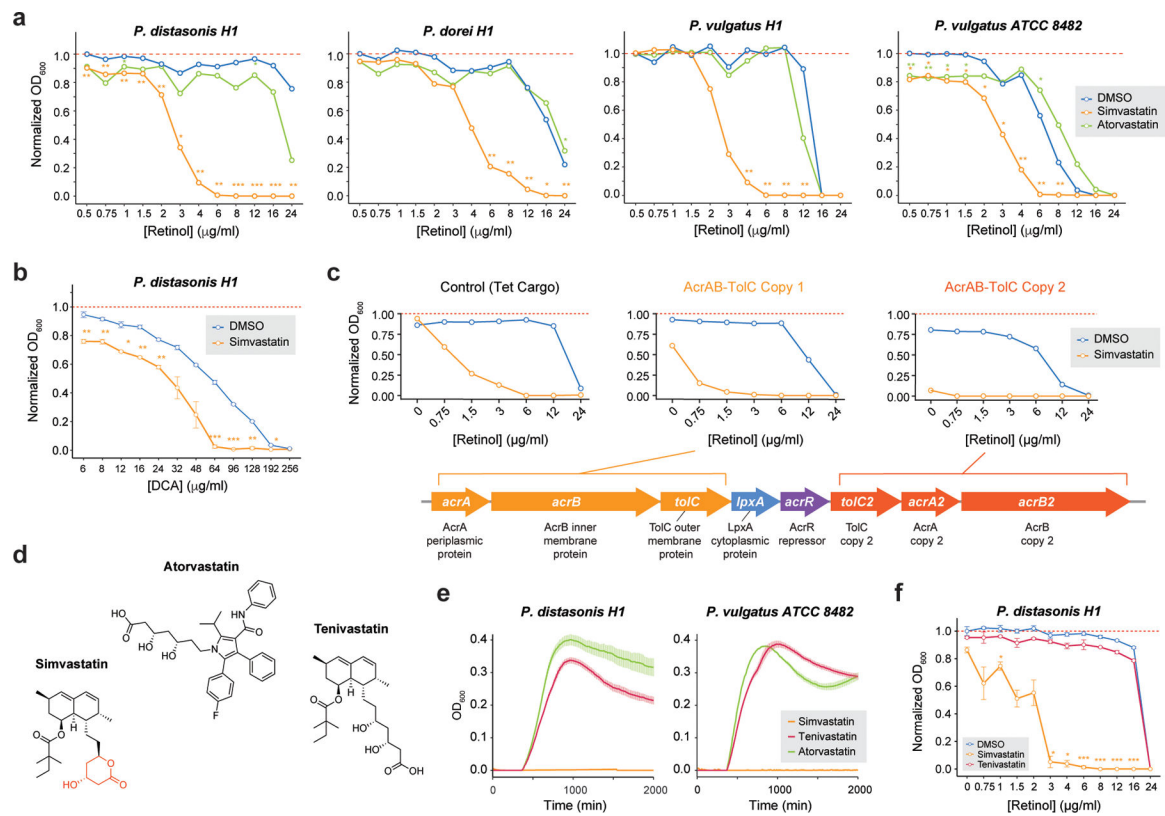


Figure 4. Statin exposure alters *Bacteroides* sensitivity to common dietary metabolites via the AcrAB-TolC efflux pump.

(a) *Bacteroidales* isolates exposed to retinol at various concentrations in the presence of 20 μM simvastatin (orange lines), atorvastatin (green lines), or vehicle control (blue lines). Graph titles indicate strain identity, with retinol concentration shown on the x-axis and growth (OD^{600} , optical density at 600 nm wavelength) relative to a vehicle control shown on the y-axis. (b) *P. distasonis* H1 exposed to various deoxycholic acid (DCA) concentrations in the presence of 20 μM simvastatin (orange lines) or vehicle control (blue lines). Bile acid concentration is shown on the x-axis, and growth relative to a vehicle control is shown on the y-axis. Standard deviation bars ($n=3$ biologically independent culture replicates per condition) are shown, and stars indicate $p_{\text{adj}} < 0.05$ (*), $p_{\text{adj}} < 0.01$ (**), and $p_{\text{adj}} < 0.001$ (***) calculated by two-sided independent t-test with Benjamini & Hochberg correction. (c) *P. vulgatus* H1 overexpressing different copies of AcrAB-TolC (see schematic) or a plasmid control exposed to different concentrations of retinol in the presence of 20 μM simvastatin ($n=3$ biologically independent culture replicates, orange lines) or vehicle control ($n=3$ biologically independent culture replicates, blue lines). Retinol concentration is shown on the x-axis, and average OD^{600} growth across replicates relative to average growth of vehicle controls is shown on the y-axis. (d) Structures of atorvastatin, simvastatin, and tenivastatin (simvastatin-hydroxy acid). The lactone ring in simvastatin is shown in red. (e) *P. distasonis* H1 and *P. vulgatus* ATCC8482 grown in liquid mGAM supplemented with simvastatin (orange line), tenivastatin (raspberry line), or atorvastatin (green line) at 100 μM concentrations. Standard error bars ($n=4$ biologically independent culture replicates per condition) for average OD^{600} growth across replicates are shown. (f) *P. distasonis* H1

retinol MIC curves in the presence of 20 μM simvastatin (n=2, orange line), tenivastatin (n=3 biologically independent culture replicates, raspberry line), or vehicle control (n=3 biologically independent culture replicates, blue line). p_{adj} values and standard deviations of average OD^{600} growth at each concentration are annotated as in **(b)**.

Author Manuscript

Author Manuscript

Author Manuscript

Author Manuscript

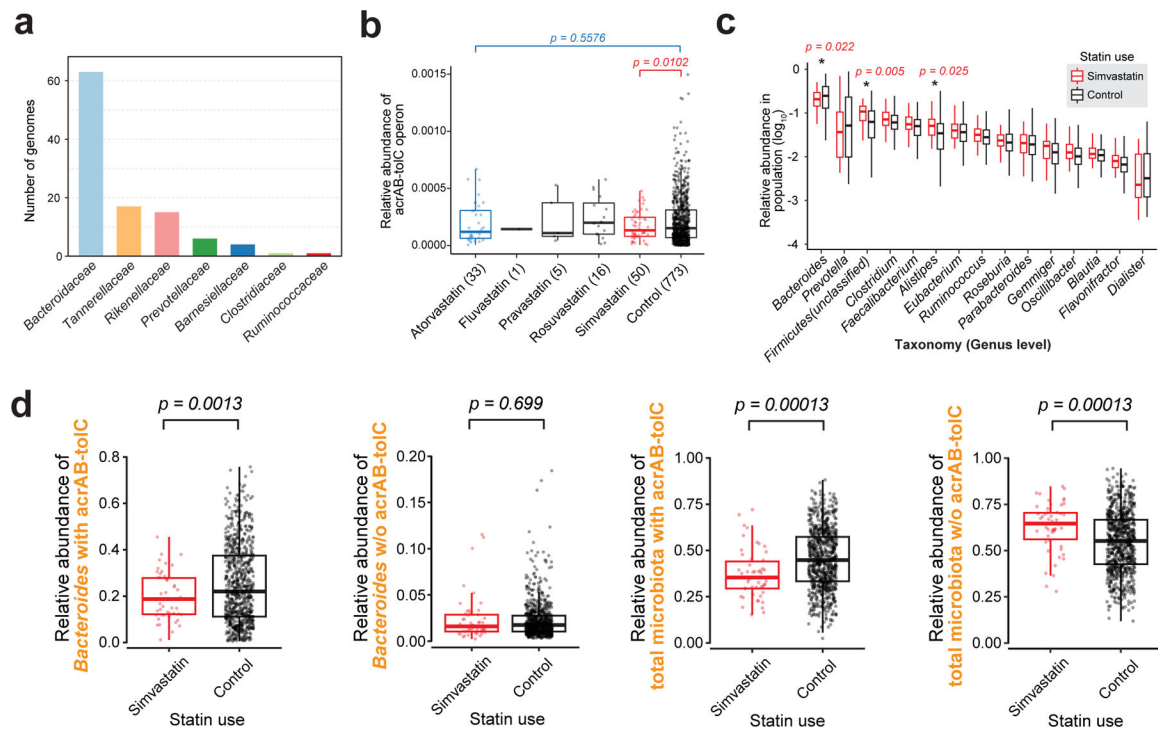


Figure 5. AcrAB-TolC is linked to gut microbiota shifts in statin-treated patient populations.

(a) The number of genomes containing *acrAB-toIC* analogs based on Ref⁶³. Bacterial family is indicated on the x-axis and by bar color. The number of *acrAB-toIC*-containing genomes within each family is indicated on the y-axis. **(b)** The relative abundance of *acrAB-toIC* within treatment groups of the BMIS cohort is shown. Statin or control cohorts are indicated on the x-axis. Simvastatin (red) and atorvastatin (blue) cohorts are highlighted, and corresponding p-values (calculated by two-sided independent t-test) are annotated with colored brackets. Each dot represents a different patient metagenome. **(c)** Relative abundance of bacterial species within the BMIS dataset, annotated using Ref⁶³. For each genus, the \log_{10} relative abundance within simvastatin-treated (red) and non-treated (black) individuals is shown as a box and whisker plot. Box hinges correspond to the 25th and 75th percentiles, and whiskers extend to values within 1.5 the interquartile range (outliers omitted). Stars indicate $p < 0.05$ (*) as calculated by two-sided independent t-test. **(d)** Relative abundance of *Bacteroides* species (left two panels) or all gut bacteria (right two panels) in simvastatin-treated and untreated individuals within the BMIS cohort. Within each panel, the x-axis indicates simvastatin (red) or control (black) treatment cohort, and relative abundances of species with or without the *acrAB-toIC* operon are labeled on the y-axis. P-values are annotated as in (b).

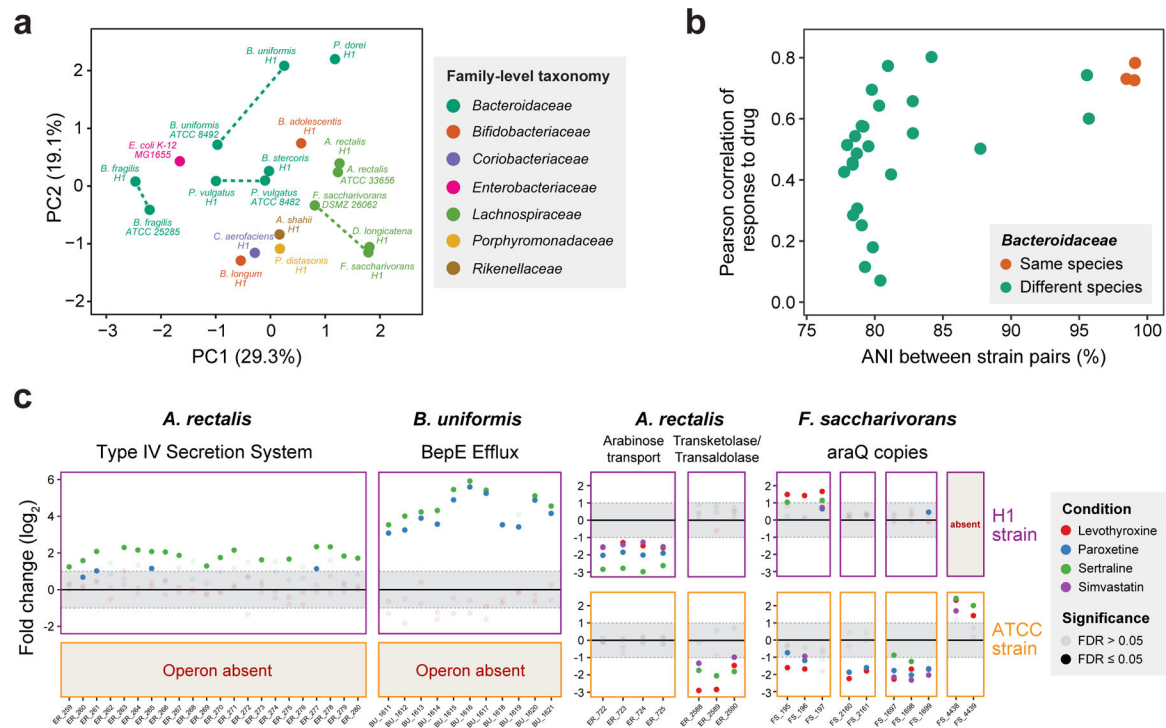


Figure 6. Diverse patterns of transcriptional response among conspecific bacterial isolates.

(a) Plot of PCoA results comparing the transcriptomic responses of tested gut bacterial isolates to top pharmaceutical compounds, using DEGRs within each drug condition as features. Variance contribution of first and second principal coordinates are shown on the x- and y- axes, respectively. Bacterial family of each isolate is indicated by color. Conspecific strains are connected by dotted lines. (b) For each possible pair of *Bacteroidaceae* strains, a comparison of average nucleotide identity (ANI, shown on x-axis) and Spearman correlation of DEGRs across all drug conditions (shown on y-axis) is shown. Each dot indicates a pairwise comparison, with color indicating whether the comparison was performed on conspecific (red) or allospecific (green) strains. (c) Differential regulation of selected operons by simvastatin (purple dots), sertraline (green dots), paroxetine (blue dots), or levothyroxine (red) dots are depicted for different conspecific strains (purple boxes depict operon expression in strain H1, yellow boxes depict operon expression in a publicly available strain). Grey dots indicate $p_{adj} > 0.05$. Species and operon identities are indicated by panel titles, and strain identity is shown on the right y-axis. $\log_2(FC)$ in gene expression as compared to a vehicle control is shown on the left y-axis and aligned gene IDs are shown on the x-axis. Absence of an operon is indicated by a beige panel with red annotation. Gray dashed lines and box indicate significance threshold of $FC > 2$.